Cr-Ga-N Materials for Negative Electrodes in Li Rechargeable Batteries: Structure, Synthesis and Electrochemical Performance

by

Miso Kim

Bachelor of Science, Materials Science and Engineering
Seoul National University, February 2004

Massachusetts Institute of Technology

Submitted to the Department of Materials Science and Engineering
in Partial Fulfillment of the Requirements for the Degree of

Master of Science

at the

Massachusetts Institute of Technology

September 2007

Signature of Author .....
Department of Material Science and Engineering
August 17, 2007

Certified by .....
Yet-Ming Chiang
Kyocera Professor of Ceramics
Thesis Supervisor

Accepted by .....
Samuel M. Allen
POSCO Professor of Physical Metallurgy
Chair, Departmental Committee on Graduate Students

Cr-Ga-N Materials for Negative Electrodes in Li Rechargeable Batteries: Structure, Synthesis and Electrochemical Performance

By

Miso Kim

Submitted to the Department of Materials Science and Engineering
in Partial Fulfillment of the Requirements for the Degree of
Master of Science in Materials Science and Engineering

ABSTRACT

Electrochemical performances of two ternary compounds (Cr_2GaN and Cr_3GaN) in the Cr-Ga-N system as possible future anode materials for lithium rechargeable batteries were studied. Motivation for this study was dealt in chapter 2 following chapter 1 that covered introduction to batteries, lithium ion batteries and anode materials for lithium ion batteries. Synthesis method with less time was attempted and factors affecting synthesis of these compounds were investigated. (Chapter 3) Through electrochemical characterization and *in-situ* XRD, practical values of electrochemical capacities were examined in comparison with theoretical capacity values (Chapter 4) and also possible reaction mechanisms of these compounds vs. Li were proposed (Chapter 5).

Thesis Supervisor: Yet-Ming Chiang
Title: Kyocera Professor of Ceramics, Department of Materials Science and Engineering

Acknowledgements

First of all, I would like to thank my advisor, Prof. Yet-Ming Chiang for his support in various ways. I'm also grateful to Chiang group members. I cannot express my gratitude enough to my loving parents and my sister for their endless love and support. I deeply appreciate my husband, Jongchul. Without him, I couldn't have completed this thesis. I also thank my friend at MIT and at FKCC for their advice and prayers. Above all, I give my thanks to Lord, my shepherd. ☺

Contents

Chapter 1 Introduction and Background 11

1.1 Batteries 11

1.2Li-ion Rechargeable batteries 13

1.3 Materials for Negative Electrodes in Li-ion Rechargeable Batteries 18

1.3.1 Lithium Metal and Cabonaceous Materials 18

1.3.2 Alternative materials for negative electrodes 19

1.4 Objective of this study 25

1.5 References 27

Chapter 2 Motivation for Cr-Ga-N system 30

2.1 Introduction 30

2.2 Gallium metal and Li-Ga alloy 30

2.3 Layered structure M_2AX 35

2.4 Selection of Cr-Ga-N system 39

2.5 Difficulties in this research 43

2.6 References 45

Chapter 3 Synthesis and structure of Cr-Ga-N system 48

3.1 Starting materials 48

3.2 GaEx samples 48

3.2.1 Experimental procedures 48

3.2.2 Results and Discussion 51

3.3 CGN samples 58

3.3.1 Experimental procedures 58

3.3.2 Results and Discussion 59
3.4 References 68

Chapter 4 Electrochemical Performances 69

4.1 Experimental procedure 69
4.2 Results and Discussion 71
4.2.1 Electrochemical performance of Cr-Ga-N materials 71
4.2.2 Possible reaction mechanisms of Cr-Ga-N materials 84
4.3 References 95

Chapter 5 Conclusion 97

List of Figures

Fig. 1.1 Representation of a battery (Daniell cell) showing the key features of a battery operation and the requirements on electron and ion conduction.[2] 12

Fig. 1.2 Comparison of the different battery technologies in terms of volumetric and gravimetric energy density.[3] 14

Fig. 1.3 Schematic representation of Li-ion rechargeable battery operation (a) (left) discharge (b) (right) charge [2, 3] 15

Fig. 2.1 Appearance of gallium metal (a) (left) typical (melted blob), (b) (right) crystallized [1] 31

Fig. 2.2 Phase equilibrium diagram of the Li-Ga system at 1atm [3] 33

Fig. 2.3 Voltage composition profile for (a) LiGa/Li and (b) Li_2Ga/Li cells [3] 34

Fig. 2.4 Unit cells of, (a) 211, (b) 312, and (c) 413 phases. Unit cells are delineated by vertical arrows labeled c. The horizontal dashed line drawn through the centers of the unit cells. [4] 35

Fig. 2.5 XRD of as-processed samples of Cr_2GaN and the same surface after exposure to the atmosphere for 24 hours at room temperature. Note emergence of Ga peaks and reduction in the peak intensities of the basal, or (0006) planes of Cr_2GaN. [12] 41

Fig. 2.6 A series of SEM images of the surface of a Cr2GaN sample exposed to the atmosphere for 50 hrs. A) Filaments observed are pure single crystal-

line Ga. B) Same as (A), but at higher magnification. C) Same as A), but at a different location, D) the sample after six months, showing marked increase in density and lengths of whiskers [12] 42
Fig. 3.1 XRD patterns of GaEx 2 sample..... 55
Fig. 3.2 XRD patterns of GaEx 3 sample..... 56
Fig. 3.3 XRD patterns of GaEx 6 sample..... 57
Fig. 3.4 XRD patterns of CGN 4 sample 63
Fig. 3.5 XRD patterns of CGN 5 sample 64
Fig. 3.6 XRD patterns of CGN 6 sample 65
Fig. 3.7 XRD patterns of CGN 7 sample 66
Fig. 3.8 XRD patterns of CGN 9 sample 67
Fig. 4.1 Voltage-capacity curve of GaEx 2 (left) and voltage-percentage of capacity curve of GaEx 2 during the first cycle (discharge in red line and charge in black line) (right) 73
Fig. 4.2 Voltage composition profile for LiGa/Li and Li_2Ga/Li..... 74
Fig. 4.3 cycle capacity vs. cycle number of GaEx 8 (before milling and GaEx 9 after milling) tested at room temperature and 37 ℃ 74
Fig. 4.4 Voltage-capacity curve of GaEx 8 before milling (up) and after milling (bottom) 75
Fig. 4.5 patterns of CGN5 after electrode casting 77
Fig. 4.6 Electrochemical test result for CGN 5. (a) Voltage-capacity curve, (b) voltage profile during the 1st cycle, and (c) cycle capacity 78
Fig. 4.7 Electrochemical test results for CGN5 at different current rate 79
Fig. 4.8 Electrochemical test results of CGN9. (a) Voltage-capacity curve, (b)

voltage-percentage capacity curve in the 1st cycle, and (c) cycle capacity vs. cycle number 82

Fig. 4.9 Electrochemical test results of CGN9 at different current rates 83

Fig. 4.10 The crystal structures of (a), (b) LiGa and (c) Li_2Ga.[1] 92

Fig. 4.11 Voltage-capacity profile of Cr2O3 [8] 93

Fig. 4.13 Voltage-percentage of capacity of GaEx2, CGN5, and CGN9 during the first cycle on the same plot 94

List of Tables

2.1 Theoretical capacity values and molar volume ratio of lithiated compound to metal of Al, Ga, Si, and Sn 32

2.2 Summary of all Mn+1AXn compounds known to date.....38

2.3 Theoretical capacities of several H-phase materials.....39

3.1 Summary of compositions, times and temperatures of runs carried out on GaEx samples.....52

3.2 Summary of heat treatment conditions for CGN samples.....60

4.1 Electrochemical capacity values of GaEx2 73

4.2 Unit cell parameter variation of CGN5 upon lithiation 92

1. Chapter 1 Introduction and Background

1.1 Batteries

Limitations of energy consumption relying on fossil fuels call for finding alternatives in energy production. In this manner, the development of electrochemical systems such as batteries, fuel cells, and electrochemical capacitors occupies public attention. Among these systems, batteries are the ones that have experienced the biggest growth in the market in the past few decades due to their various practical applications and advantages.[1, 2]

Batteries are composed of one or several electrochemical cells that are electrically connected in series and/or in parallel to provide the required voltage and capacity, respectively. Each cell consists of positive and negative electrodes separated by electrolyte solutions, which enable ion transfer between two electrodes. In batteries, electrical energy is generated by conversion of chemical energy via redox reactions that occur at the electrode/electrolyte phase boundary. Once electrodes are connected externally, the chemical redox reactions proceed at both electrodes, and electrons, therefore, are liberated so that current flows. The amount of electrical energy (Wh/kg) is typically expressed either per unit of weight (Wh/kg) (specific energy) or per unit of volume (Wh/l) (energy density) and is a function of voltage (V) and capacity (Ah/kg), both of which are strongly related to the chemistry of selected systems. This implies that selection and control of chemical reaction systems is a significant matter in order to obtain desired electrical properties. Batteries are regarded as closed systems in that

energy storage and conversion take place in the same compartment since both negative and positive electrodes play main roles not only as charge-transfer media but also as active masses in the redox reaction. The requirements on electron and ion conduction in battery systems are shown in Figure 1.1 along with basic battery operation.

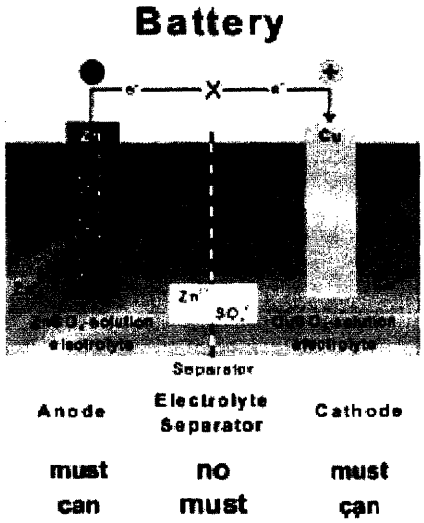

	Anode	Electrolyte Separator	Cathode
Requirements on electron conduction:	must	no	must
Ion conduction:	can	must	can

Fig. 1.1 **Representation of a battery (Daniell cell) showing the key features of a battery operation and the requirements on electron and ion conduction.[2]**

As illustrated above, the basic elements comprising a battery are anode, cathode, electrolyte, and sometimes separator. The anode is the negative electrode of a cell associated with oxidative chemical reactions that release electrons into the external circuit. The cathode is the positive electrode of a cell associated with reductive chemical reactions that gain electrons from the external circuit. The electrolyte is the material that provides pure ionic conductivity between the positive and negative electrodes of a cell. The separator is a physical barrier between the positive and negative electrodes to prevent a battery (cell) from shorting.

Typically, batteries are divided into three general categories: primary batteries, secondary/rechargeable batteries and specialty batteries. Primary batteries are assembled in the charged state and discharged during use and then discarded. Secondary/ rechargeable batteries are the cells that can be discharged and then restored to their original charged condition by reversing electric current flow. Since rechargeable batteries are usually assembled in the discharged state, they have to be charged before use. Specialty batteries are primary batteries designed for specific purposes such as military and medical use.

1.2Li-ion Rechargeable batteries

Among numerous batteries, the lithium rechargeable battery has become the most indispensable due to the increasing demand of portable electronic devices such as laptop computers and cellular phones. Compared to other rechargeable battery systems, lithium rechargeable batteries are very attractive in that they provide high energy density, flexible and light weight design, and longer lifespan. (Figure 1.2) [3]

The original motivation for Li-based batteries is due to the fact that lithium is the most electropositive (-3.04 V versus standard hydrogen electrode) and lightest metal, which gives design flexibility and energy density. Based on this fact, the first commercial assembly of lithium primary cells using lithium metal as an anode was made in the

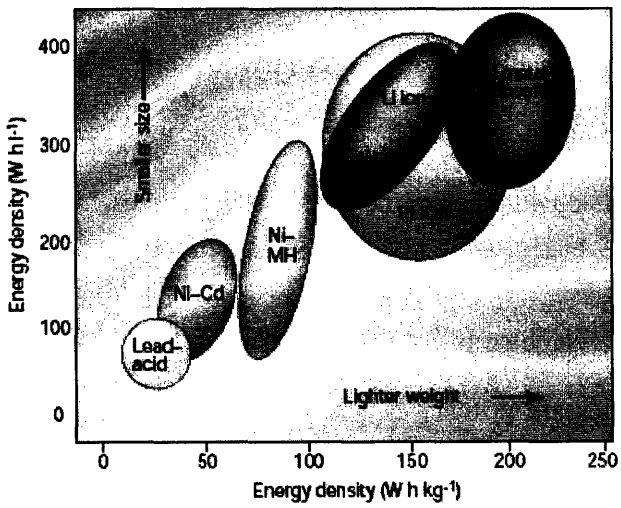

Fig. 1.2 Comparison of the different battery technologies in terms of volumetric and gravimetric energy density.[3]

1970s, followed by rapid application in watches, calculators and so on due to its large capacity and variable discharge rate. Intercalation compounds such as TiS_2 were investigated as positive electrode materials that react with alkali metals reversibly. However, the problem of uneven dendritic lithium growth during subsequent charging and discharging from a combination of a lithium metal and liquid electrolyte, which might result in explosion hazards, restricted the use of lithium metal and assembly of Li metal based batteries. Over the following years, oxides such as V_6O_{13} and then Li_xMO_2 (M=Co, Ni, or Mn), offering higher capacities and voltages have been discovered as positive electrode materials. As anode materials, Al alloys were investigated to replace Li metal but unsuitable to use due to extreme change in volume during cycling, leading to cycling fade. The idea of using insertion materials in which Li is present in its ionic state rather than its metallic state so that safety problem can be lessened was proposed and active research on discovery of appropriate insertion materials such as lithium alloys and transition metal oxides was done. Eventually, in 1991, Sony commercialized

the first Li-ion rechargeable batteries, $C/LiCoO_2$, also called rocking chair batteries, which provide potential exceeding 3.6V and gravimetric energy density around 120-150 Wh/kg. This attributed to the discovery of highly reversible, low voltage lithium intercalation-deintercalation processes in carbonaceous materials. This type of battery is still the main source powering today's high performance portable electronic devices.[3]

In lithium-ion rechargeable batteries as well as in other batteries, charge/discharge processes occur toward the direction that reduces the potential at each electrode. Upon discharge, Li dissociates into Li ion and electrons at the anode (oxidation) as shown in the following equation.

$$xLi \Leftrightarrow xLi^{+} + x\, e^{-} \qquad \text{(Equation 1.1)}$$

Li ions are liberated from the anode side and swim through the electrolyte toward the cathode while at the same time, electrons from the anode side move through the external circuit to the cathode. (Figure 1.3a) During charge, the potential of the cathode is heightened by applying external power source so that Li ions and electrons move back to the anode through the electrolyte and external circuit, respectively. (Figure 1.3b)

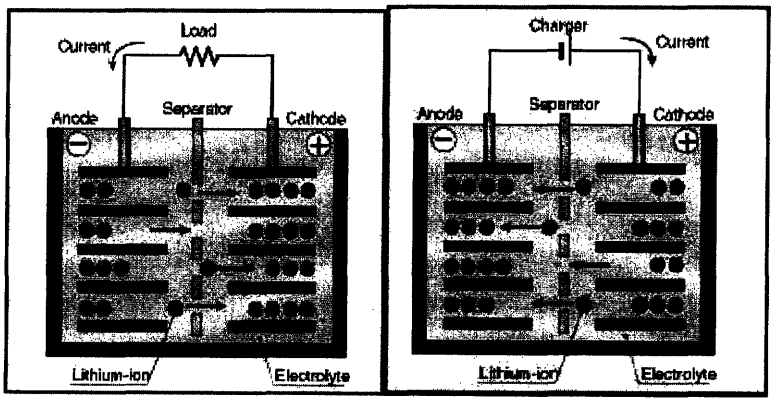

Fig. 1.3 **Schematic representation of Li-ion rechargeable battery operation (a) (left) discharge (b) (right) charge [2, 3]**

For the sake of better understanding, it is necessary to define several essential properties in Li-ion rechargeable batteries: voltage, capacity, energy density, power density, and cycle life.

In lithium-ion rechargeable batteries, a voltage is established by the difference in the chemical potential of Li^+, μ_{Li+}, between the anode and cathode. This is expressed in equation (1.2)

$$V = -\frac{(\mu_{Li}^{cathode} - \mu_{Li}^{anode})}{nF} \qquad \text{(equation 1.2)}$$

where V = voltage of a battery

$\mu_{Li}^{cathode}$ = chemical potential of Li^+ at the cathode

μ_{Li}^{anode} = chemical potential of Li^+ at the anode

n = the number of moles of Li that can participate in the electrochemical reaction

F = Faraday constant = 96,485 C/mole

The minus sign arises because anode and cathode accommodate Li ions at high and low potential, respectively. When no external current flows, the voltage is called open-circuit voltage, which is usually close to the thermodynamic voltage of the system. Closed-circuit voltage refers to the voltage of a battery when the battery is in operation, producing current that flows into the external circuit.

The capacity of a battery is the total quantity of electricity involved in the

electrochemical reaction and defined in terms of coulombs [C] or ampere-hours [Ah]. The theoretical specific gravimetric capacity of an electrode can be calculated by the expression below:

$$Q\ [mAh/g] = \frac{n*96485C/mol}{M[g/mol]} X \frac{1000mAh/Ah}{3600\sec} \qquad \text{(Equation 1.3)}$$

where Q = theoretical capacity of an electrode

n = number of Li ions involved in the reaction per mole of active electrode material M = molar weight of active material

Depending on cases, volumetric capacity [mAh/cm^3] is also used.

Energy density is defined as the amount of energy per unit weight or volume. As previously mentioned, energy density is a function of capacity and voltage as expressed by equation 1.4.

$$E\ [Wh/g \text{ or } Wh/cm^3] = Q\ [Ah/g \text{ or } Ah/cm^3] \times V\ [V] \qquad \text{(Equation 1.4)}$$

where Q = Capacity

V = Battery voltage

Power density is defined as battery power per unit weight or volume and expressed in units [W/kg] or [W/l]. It can be calculated by the product of current density, I [A/kg] and the battery voltage [V]. Power density can also be regarded as energy density per unit time.

Cycle life is also of importance in Li-ion rechargeable batteries. Cycle life, also called cyclability refers to a large number of charge/discharge cycles with little or no capacity drop that batteries can withstand. Commercial batteries should be capable of completely discharging their energy and then fully recharging at least 300 times with capacity drop less than 20 %.

In general, the desirable batteries are the ones with high voltage (high power density) and large capacity (higher energy density). In addition, low cost production, safety and fast charging time are also significant factors in considering rechargeable batteries.

1.3 Materials for Negative Electrodes in Li-ion Rechargeable Batteries

1.3.1 Lithium Metal and Cabonaceous Materials

As previously mentioned, development of lithium rechargeable batteries originates from the characteristics of Li metal: the most electropositive and lightest metal. Hence, in the beginning, elemental lithium metal was used as an anode but soon discarded due to severe safety problems such as explosion hazards resulting from dendritic growth upon cycling. Currently carbonaceous materials have been employed in many commercial batteries since the first commercialization by Sony in 1991. Up to 1 atom of lithium per six carbon atoms can be intercalated into graphite (LiC_6), giving a maximum theoretical capacity of 372 mAh/g at relatively low voltage (~0.1V) relative to Li metal. Practically, capacity values between 300-350 mAh/g are obtained. Although carbonaceous materials

take up and release Li^+ ions quite reversibly over 500 cycles and can be produced at low cost, their gravimetric capacity of 372mAh/g is small compared to the theoretical gravimetric capacity value of Li metal (3829mAh/g). Accordingly, much effort has been devoted to find carbon replacement materials while research on improvement of carbon negative electrode performance through chemical or physical modification has been carried out simultaneously. Several proposed alternative materials for negative electrodes in Li-ion rechargeable batteries are treated in the next section along with advantages and drawbacks for each.[3, 4]

1.3.2 Alternative materials for negative electrodes

Li-metal alloys

Instead of using Li metal as an anode, researchers have investigated a series of alloys and compounds of lithium, which not only have potential values just slightly above that of lithium metal but also are expected to exhibit very large theoretical capacity values (Table 1.1). Initially, interest was placed on high temperature Li batteries with Li-Al alloys as negative electrodes and later on ambient temperature Li-ion rechargeable batteries consisting of numerous systems such as Li-Sn and Li-Si. Although Li metal alloys are attractive in terms of gravimetric capacity, they suffer from poor cycling due to drastic volume change upon insertion and removal of Li during cycling. As shown in Table 1.1, the volume change is typically on the order of 100%. This colossal change in volume results in mechanical stress and strain inside electrode microstructure, causing disintegration and loss of electrical contacts between particles upon cycling. Many

efforts have been devoted to find a way to lesson the volume change and to understand the mechanism of reaction with Li upon cycling in order to improve cyclability and take advantage of the large gravimetric capacity of these systems. [4]

Oxides

Considerable interest has grown in using convertible oxide materials as anodes since Fuji film announced its decision to use amorphous tin composite oxides (ATCO) in negative electrodes. These oxides react reversibly with lithium at about 0.5V and the reversible capacities are larger than 600 mAh/g and 2200 Ah/l, which doubles the specific capacity of graphite (372 mAh/g and 1200 Ah/l). Several research groups have investigated the lithium reactivity mechanism in these composites upon discharge/charge mainly from *In situ* X-ray diffraction analysis. According to initial work on non-crystalline tin oxides, during the first charging cycle, oxides are decomposed by lithium to form intimately mixed Li_2O and metallic Sn. This initial irreversible reaction is followed by Li alloying reaction with Sn to form nanodomains of $Li_{4.4}Sn$ embedded within the Li_2O matrix. These scenarios are summarized in Table 1.2 for some tin oxide materials.

Initial		Fully discharged		Charged again
4.4Li + Sn	->	Li4.4Sn	⇔	4.4Li + Sn
6.4Li + SnO	->	Li2O + Li4.4Sn	⇔	4.4Li + Sn
8.4Li + SnO2	->	Li2O + Li4.4Sn	⇔	2Li2O + 4.4Li + Sn

Table 1.2

Recently, there are two distinguishable approaches to describe this mechanism of

reaction. One is that other elements that are produced from the reaction of Li-Sn are regarded as mere "spectator" to stay electrochemically inactive while electroactive Li-Sn alloys are mechanically dispersed. Another approach is that the dispersing matrix and the Sn atoms interact with each other strongly. The latter approach has been reinforced by the application of different spectroscopy such as Mossbauer spectroscopy that can identify the non-crystalline structure of products better than diffraction techniques. A major problem with oxides is that the electrode is subject to an unacceptably large irreversible capacity loss, which is attributed to the inability of the lithium trapped within the Li_2O matrix to partake in the electrochemical reaction. Poor long-term cyclability is also a problem to overcome. [5-9]

Transition metal oxides, M-O (where M = Co, Ni, Re, Cu, Mn et cetera), were also proposed and have been studied as alternatives for negative electrodes in lithium ion rechargeable batteries. These binary oxides exhibit capacities two to three times those of carbons with 100% capacity retention up to 100 cycles. In these cases, transition metals, as indicated by M above, are known to not alloy with Li. Similar to tin oxides, these oxides are reduced to Li_2O and metal nanoparticles during the first discharge at quite a low voltage. Unlike the tin oxide case where Li alloys mostly with Sn within a matrix of Li_2O in subsequent cycles, decomposition and formation of Li_2O are known to occur upon further cycling, demonstrating very reversible capacities. M.N.Obrovac et al. verified the following scheme.

First discharge α-CoO + 2Li -> Co + Li_2O (Equation 1.5)

Further cycling Co + Li_2O $\Leftrightarrow$ β-CoO + 2Li (Equation 1.6)

In addition, such materials as NiO, FeO, Cu_2O, Cr_2O_3, α-$LiFeO_2$, β-Li_5FeO_4 have

been reported to show quite reversible capacities through the reaction described above. Although transition metal oxides reduced to Li_2O and metal demonstrate high reversible capacities compared to graphite with reasonable cycle life, the huge irreversible capacity loss during the first discharge cycle obstructs commercial use of these materials.[10-15]

In terms of the type of reactions versus lithium, there is another kind of transition metal oxide that is considered to be an intercalation electrode material. These include not only transition metal oxides with spinel structure, such as Fe_3O_4, Mn_3O_4, Co_3O_4, and $Li_4Ti_5O_{12}$ but also anatase TiO_2. As in the case of intermetallic alloys that will be discussed later in this chapter, these oxides typically exhibit capacities lower than that of carbon at a much higher voltage relative to Li metal, giving a lower voltage battery. $Li_4Ti_5O_{12}$, for example, shows a capacity value of about 150 mAh/g at a voltage plateau of 1.5V. Yet, these materials are interesting potential candidates for negative electrode materials in that the combination of these anode materials with high voltage positive electrodes is seen as a possibility to compensate the higher working voltage of the intercalation compounds versus lithium.[14-17]

Intermetallic alloys

One of the most common approaches to alleviate the problem of alloy expansion is to embed an "active" binary intermetallic electrode in a composite matrix. As discussed already, a well-known representative of such systems is tin oxide system where Li-Sn alloys are created within an electronically insulating Li_2O matrix during the

electrochemical reaction with lithium. Considerable research has also been undertaken on intermetallic composite structures such as $FeSn_2$ or $CoSb_3$ in which active Li_xSn and Li_3Sb cycle within inactive Fe and Co matrices, respectively. In these systems, the large structural differences exist between original (parent) and lithiated compounds, limiting the reconstruction of the parent structure during delithiation. The large 1^{st}-cycle irreversible capacity loss is also problematic. [18-21]

Intermetallic compounds such as Cu_6Sn_5, InSb, Cu_2Sb have been proposed by Thackeray et al. for negative electrode materials as a new approach to alleviate the problems of alloy expansion. The selection of these compounds was based on the "structural compatibility" of the original compound with the lithiated product phase. These intermetallic alloys undergo reversible process of lithium insertion and metal intrusion on discharge. In this process, a strong structural relationship exists between a parent binary intermetallic electrode, MM', in which M and M' are different metal atoms, and a lithiated Li_xMM' product and therefore, less volume change upon occurs in these materials upon cycling than in lithium metal alloy expansion. Cu_6Sn_5, for example, reacts with lithium as illustrated in Equation 1.7.

$$10Li + Cu_6Sn_5 \Leftrightarrow 5Li_2CuSn + Cu \qquad \text{(Eqaution 1.7)}$$

In this case, nickel-arsenide structure of Cu_6Sn_5 is strongly related to the lithiated zinc-blend structure and thus, the volume expansion of the copper-tin structure during this reaction is approximately 59%, which is much less than those of lithium-metal alloys. Binary Sn-M system where M equals to Co, Ni, In, Pb also belongs to these

intermetallic compounds. These intermetallic alloy materials demonstrate reasonable cycle life through a reversible process as explained. However, they exhibit capacities lower (250-300 mAh/g) than that of carbon at a much higher voltage relative Li metal, producing lower voltage battery and still suffer from poor cycle life. [18, 19, 21, 22]

Metal Nitrides

Ternary lithium transition-metal nitrides have also achieved researchers' interest as new potential class of anode materials. Nashijima et al. first introduced ternary lithium transition-metal nitrides such as Li_3FeN_2 and Li_7MnN_4, which have the general formula of $Li_{2n-1}MN_n$. This group of nitrides is known to have cubic antifluorite-type structure and undergo reconstitution (addition) reactions with stoichiometric changes of Li. There materials show quite good rechargebility with capacity value of 150-200 mAh/g. A second group of ternary lithium transition-metal nitrides, $Li_{3-x}M_xN$ where M stands for Cu, Ni, and Co, have also been investigated for their electrochemical properties. These nitrides are isostructural to the hexagonal Li_3N where the transition metal substitutes for Li in between Li_2N layers. $Li_{2.6}Co_{0.4}N$ was reported to exhibit good cycling stability and high capacity of about 760 mAh/g at an average discharge potential of about 0.8 V vs. Li. In spite of large, stable and reversible capacity, the commercialization of these nitride materials is constrained by their moisture sensitivity and the requirement of a predelithiation step before use as negative electrodes in Li-ion batteries. [11, 23, 24]

There has been also some interest in the use of some nitrides such as Sn_3N_4, tin subnitrides, InN, Zn_3N_4, silicon tin oxynitrides, Cu_3N, and Ge_3N_4 as possible negative

electrode reactants in lithium cells. These materials were found to react with lithium in a two-step process similar to the one observed in tin-based amorphous composite oxides. Through an irreversible conversion reaction, a Li_3N matrix and an electrochemically active metal M are generated. The subsequent metal alloying and dealloying reactions with lithium the reversible capacity. These two steps are depicted in Equation 1.8 and 1.9, respectively.

$$M_xN_y + 3yLi^+ + 3ye^- \rightarrow xM + yLi_3N \qquad \text{(Equation 1.8)}$$

$$M + zLi^+ + ze^- \Leftrightarrow Li_zM \qquad \text{(Equation 1.9)}$$

Similar to the case of tin-based amorphous composite oxides, the formation of Li_3N matrix attributes to the irreversible capacity loss in the first cycle of these materials. More detailed discussion of the reaction mechanism can be found in Reference [23, 24].

1.4 Objective of this study

As seen in the previous section, there are various approaches to find the materials that can displace the carbon materials that are currently used for negative electrodes in lithium-ion rechargeable batteries. Unfortunately, none of these is yet sufficiently better to be a widely-used alternative negative electrode material. In this study, we investigated a new class of materials as possible anode reactants, based on these materials' particular structure and properties. Detailed motivation for selecting one specific system among these structure materials is presented in Chapter 2. Chapter 3 covers experimental procedures, results, and discussion regarding synthesis. Several samples of interest that consist of ternary and binary Cr-Ga-N phases were produced. With these samples, electrochemical tests were implemented in order to see if these

materials are promising as future anode materials in Li-ion rechargeable batteries. The detailed procedure and results are described in Chapter 4, followed by reaction mechanism analysis on each sample. *In-situ* X-ray diffraction method was useful to verify which proposed mechanism would be the most feasible one for each sample. Overall, our main goal lies in finding out if and how the phases of Cr-Ga-N system would react with lithium electrochemically.

1.5 References

1. Whittingham, M.S., R.F. Savinell, and T. Zawodzinski, *Introduction: Batteries and Fuel Cells.* Chemical Reviews, 2004. **104**(10): p. 4243-4244.
2. Winter, M. and R.J. Brodd, *What Are Batteries, Fuel Cells, and Supercapacitors?* Chemical Reviews, 2004. **104**(10): p. 4245-4270.
3. Tarascon, J.M. and M. Armand, *Issues and challenges facing rechargeable lithium batteries.* Nature, 2001. **414**(6861): p. 359-367.
4. Dahn, J.R., *Carbon and graphites as substitutes for the lithium anode.* Industrial Chemistry Library, 1994. **5**.
5. Courtney, I.A. and J.R. Dahn, *Electrochemical and in situ X-ray diffraction studies of the reaction of lithium with tin oxide composites.* J. Electrochem. Soc., 1997. **144**: p. 2045-2052.
6. Idota, Y., et al., *Tin-Based Amorphous Oxide: A High-Capacity Lithium-Ion-Storage Material.* Science, 1997. **276**(5317): p. 1395-1397.
7. Yang, J., M. Winter, and J.O. Besenhard, *Small particle size multiphase Li-alloy anodes for lithium-ionbatteries.* Solid State Ionics, 1996. **90**(1-4): p. 281-287.
8. Courtney, I.A., W.R. McKinnon, and J.R. Dahn, *On the Aggregation of Tin in SnO Composite Glasses Caused by the Reversible Reaction with Lithium.* Journal of The Electrochemical Society, 1999. **146**(1): p. 59-68.
9. Courtney, I.A. and J.R. Dahn, *Key Factors Controlling the Reversibility of the Reaction of Lithium with SnO[sub 2] and Sn[sub 2]BPO[sub 6] Glass.* Journal of The Electrochemical Society, 1997. **144**(9): p. 2943-2948.
10. Badway, F., et al., *Metal Oxides as Negative Electrode Materials in Li-Ion Cells.*

Electrochemical and Solid-State Letters, 2002. **5**(6): p. A115-A118.

11. Cabana, J., et al., *Antifluorite-Type Lithium Chromium Oxide Nitrides: Synthesis, Structure, Order, and Electrochemical Properties.* Inorganic Chemistry, 2004. **43**(22): p. 7050-7060.

12. Cava, R.J., D.W. Murphy, and S.M. Zahurak, *Lithium insertion in Wadsley-Roth phases based on Niobium oxide.* J. Electrochem. Soc., 1983. **30**: p. 2345-2351.

13. Obrovac, M.N., et al., *The Electrochemical Displacement Reaction of Lithium with Metal Oxides.* Journal of The Electrochemical Society, 2001. **148**(6): p. A576-A588.

14. Poizot, P., et al., *Electrochemical reactivity and reversibility of cobalt oxides towards lithium.* C.R. Acad. Sci. II, 2000: p. 681-691.

15. Poizot, P., et al., *Nano-sized transition-metal oxides as negative-electrode material for lithium-ion batteries.* Nature, 2000. **407**: p. 496-499.

16. Yuan, Z., et al., *Synthesis and electrochemical performance of nanosized Co3O4.* Materials Chemistry and Physics, 2003. **79**(1): p. 1-4.

17. Dong, W., D.R. Rolison, and B. Dunn, *Electrochemical properties of high surface area vanadium oxides aerogels.* Electrochem. Solid State Lett., 2000. **3**: p. 457-459.

18. Benedek, R. and M.M. Thackeray, *Lithium reactions with intermetallic-compound electrodes.* Journal of Power Sources, 2002. **110**(2): p. 406-411.

19. Fransson, L.M.L., et al., *Structural Transformations in Intermetallic Electrodes for Lithium Batteries.* Journal of The Electrochemical Society, 2003. **150**(1): p. A86-A91.

20. Thackeray, M.M., et al., *Structural considerations of intermetallic electrodes for*

lithium batteries. Journal of Power Sources, 2003. **113**(1): p. 124-130.

21. Vaughey, J.T., et al., *Structural and mechanistic features of intermetallic materials for lithium batteries.* Journal of Power Sources, 2001. **97-98**: p. 194-197.

22. Kepler, K.D., J.T. Vaughey, and M.M. Thackeray, *LixCu6Sn5 (0<x<13): an intermetallic insertion electrode for rechargeable lithium batteries.* Electrochem. Solid State Lett., 1999. **2**: p. 307-307.

23. Cabana, J., et al., *Oxynitrides as Electrode Materials for Lithium-Ion Batteries.* Journal of The Electrochemical Society, 2005. **152**(11): p. A2246-A2255.

24. Shodai, T., Y. Sakurai, and T. Suzuki, *Reaction mechanisms of Li2.6Co0.4N anode material.* Solid State Ionics, 1999. **122**(1-4): p. 85-93.

2. Chapter 2 Motivation for Cr-Ga-N system

2.1 Introduction

As previously shown in Chapter 1, numerous systems other than graphitic carbons, such as oxide electrodes and intermetallic alloy electrodes have received a great deal of attention. However, none of them are sufficiently satisfying yet to be able to replace lithium-carbon electrodes. In this study, we propose Cr_2GaN as one of new class anode materials for new lithium ion batteries. The initial motivation originates from the special characteristics of gallium metal as well as the laminate structure of Cr_2GaN yielding attractive properties. Our basic idea is that gallium, in the layered structure of Cr_2GaN, would take an active role in the reaction with lithium either through intercalation or alloying. Although we put our interest initially in Cr_2GaN only, difficulties in synthesis of single phase Cr_2GaN resulted in the samples composed of several Cr-Ga-N phases and thus, we extended our interest to synthesis and electrochemical performances of general Cr-Ga-N systems. More detailed features and explanation about each of these will be described in the following sections.

2.2 Gallium metal and Li-Ga alloy

Gallium is the chemical element of silvery metal that has the symbol of Ga, number 31 in the periodic table. This element has several peculiar characteristics compared to other typical "metals": gallium is a brittle solid at low temperatures but solidifies at slightly above room temperature (29.8 C), which allows this metal to be melted even in the hand.

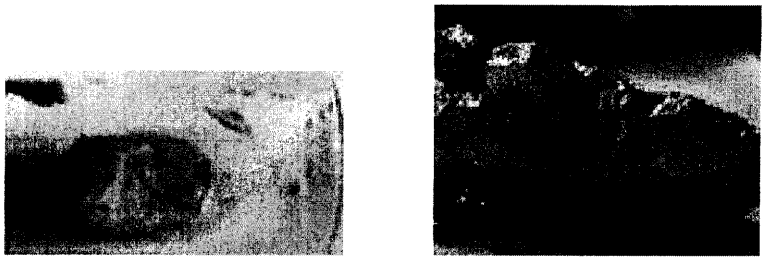

Fig. 2.1 **Appearance of gallium metal (a) (left) typical (melted blob), (b) (right) crystallized [1]**

Gallium also expands by 3.1% when solidified and this is why it should be kept neither in glass nor in metal containers. In addition, unlike mercury that is also a low melting point metal, gallium wets glass and skin, making it mechanically more difficult to handle together with low melting temperature near room temperature. Gallium also alloys with other metals very easily, attacking most other metals by diffusing into their metal lattices. [1]

Owing to these characteristics, gallium seems to us very attractive as a component as an electrochemically active material. Although it is hard to handle gallium due to its low melting point, the fact that gallium exists usually in liquid state gives the possibility that ductility might be maintained during cycling since a liquid has high surface tension but has properties equal to those of a solid. If so, this will help the system of use react very reversibly, ultimately contributing to reducing irreversibility cycling fade.

Furthermore, when compared to other well known lithium metal alloys such as Li-Sn and Li-Si, lithiated compounds of gallium show quite comparable values in terms of theoretical electrochemical capacity value by calculation. A list of numbers regarding

Table 2.1 Theoretical capacity values and molar volume ratio of lithiated compound to metal of Al, Ga, Si, and Sn [2]

Metal	MW (g/mole)	Density (g/cm3)	Molar Volume (cm3/mole of metal)	Lithiated Cmpnd	MW (g/mole)	Density (g/cm3)	Molar Volume (cm3/mole of metal)	Average Voltage (against Li)	Theor. Weight Capacity (Ah/kg of starting metal)	Theor. Volume Capacity (mAh /cm3 of starting metal)	Lithiated Cmpnd to Metal Molar Volume Ratio
Al	26.98	2.7	9.99	LiAl	33.92	1.741	19.48	0.36	993.5	2683	1.95
				Li9Al4	170.4	1.269	33.57	??	2235.5	6035.7	3.36
				Li3Al	74.79	1.484	50.4	??	2980.6	8047.6	5.05
Ga	69.72	5.91	11.8	Li5Ga4	313.59	3.804	20.61	??	480.6	2840.3	1.75
				Li2Ga	83.6	2.923	28.6	??	769	4544.5	2.42
				Li3Ga2	160.26	3.479	23.03	??	576.7	3408.4	1.95
				LiGa	76.66	4.259	18	??	384.5	2272.2	1.53
Si	28.09	2.33	12.06	Li12Si7	279.89	1.526	26.2	??	1635.9	3811.6	2.17
				Li21Si8	370.45	??	??	0.158	2505	5836.6	??
				Li13Si4	202.58	1.25	40.52	0.158	3101.4	7226.2	3.36
				Li21Si5	286.19	1.197	47.82	0.2	4008	9338.5	3.97
Sn	118.69	7.31	16.24	Li5Sn2	272.09	3.513	38.73	0.485	564.6	4127.3	2.39
				Li13Sn5	683.68	3.466	39.45	0.485	587.2	4292.4	2.43
				Li7Sn2	285.97	2.957	48.35	0.385	790.5	5778.2	2.98
				Li22Sn5	746.15	2.562	58.25	0.385	993.7	7264.1	3.59

theoretical weight and volume capacity and volume change are calculated, based on the Li-Ga phase diagram and presented in Table 2.1. Taking a look at the Li-Ga phase diagram (Figure 2.2) [3] tells us that there are several capacity-wise attractive binary Li-Ga alloys. Li_2Ga, for example, could reach a reversible capacity of 769 mAh/g theoretically, which is a value about twice the maximum graphite capacity. In addition to theoretical capacity, relatively small volume change compared to Li-Sn alloy is expected, supporting gallium as an alternative for negative electrode material in Li rechargeable batteries. Large volume expansion during lithiation is one of the most significant problems that most alloys and oxides undergo during operation since it leads to strain in microstructure and fractures, loss of electronic contact, and thus cycling capacity fade as previously mentioned in Chapter 1.

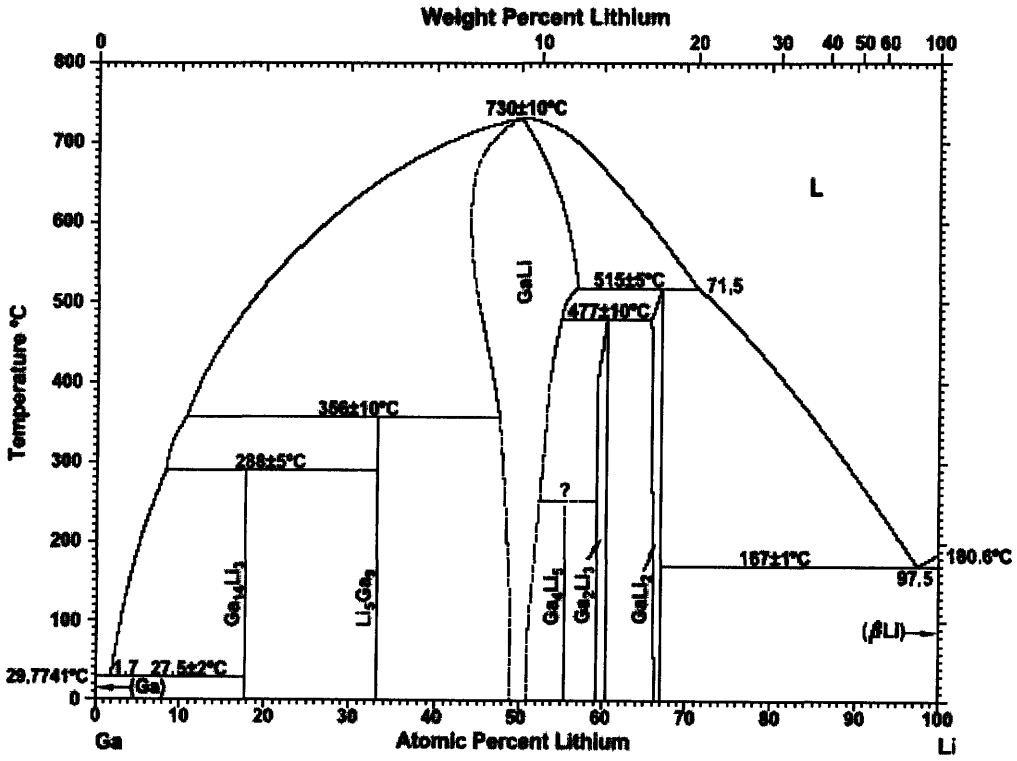

Fig. 2.2 Phase equilibrium diagram of the Li-Ga system at 1atm [3]

Recently, J.M Tarascon group reported the electrochemical performances of Li-Ga alloy vs. Li with structural change. In their study [3], Li-Ga alloy such as Li_2Ga_7, Li_2Ga and LiGa were synthesized by ball milling gallium ingots and lithium powder after considering gallium's low melting point, tested in potentiodynamic mode and analyzed through in-situ X-ray experiment. These alloys demonstrate up to the value of 400 mAh/g in terms of Li storage and undergo structural transition (Li_2Ga ⇔ LiGa ⇔

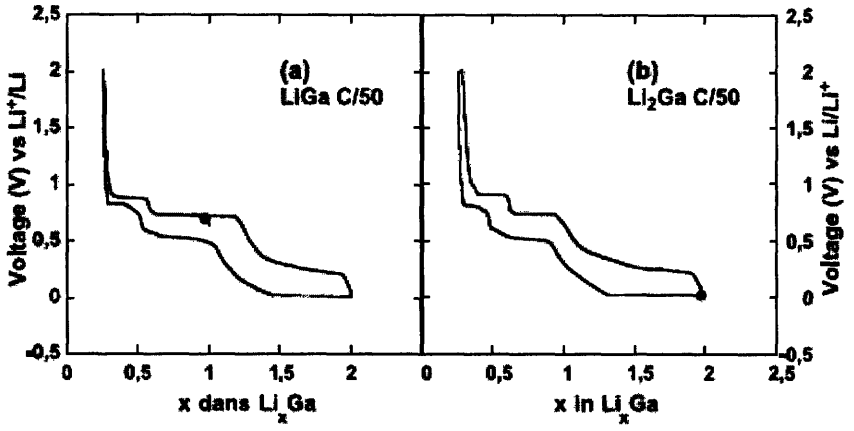

Fig. 2.3 **Voltage composition profile for (a) LiGa/Li and (b) Li_2Ga/Li cells [3]**

Li_2Ga_7) quite reversibly. The three voltage plateaus that appeared in both discharge and charge states are regarded as evidence for this structural change. (Figure 2.3) In this report, especially, the transition from Li_2Ga to LiGa is noticeable in that it is a Li-driven transformation from 2D structure (Li_2Ga) to 3D structure (LiGa). Since gallium is anticipated to be the main active material in our experiment, this structural transition phenomenon seems also to be strongly related to our experimental result and will be discussed in more detail in later chapters together with our results.

Not many studies on electrochemical performance of gallium metal or lithium-gallium

alloys have been undertaken so far. It is, therefore, also a good opportunity to investigate characteristics of gallium or lithium gallium as candidate anode materials.

2.3 Layered structure M_2AX

A family of compounds possessing an approximate $M_{n+1}AX_n$ chemistry, where M is an

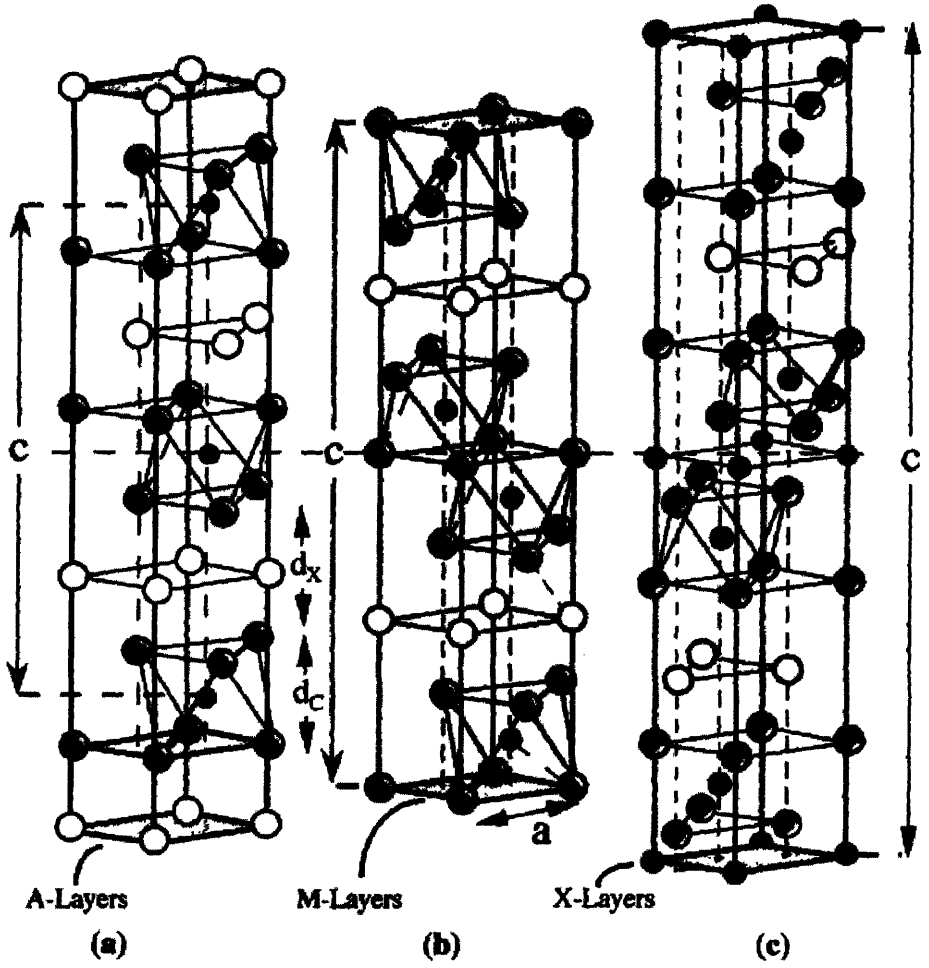

Fig. 2.4 **Unit cells of, (a) 211, (b) 312, and (c) 413 phases. Unit cells are delineated by vertical arrows labeled c. The horizontal dashed line drawn through the centers of the unit cells. [4]**

early transition metal, A is an A-group element (mostly IIIA and IVA) and X is either C and/or N, is identified and shown to have unusual combination of both metallic and ceramic properties. The $M_{n+1}AX_n$ phases, also called H-phases, have basically layered hexagonal structures where almost close-packed layers of M are interleaved with layers of pure group A-element, with X atoms filling the octahedral sites between the former. M_2AX phases, for instance, are layered and hexagonal with M_2X layers interleaved with layers of pure A while M_3AX_2 has the same structure but with M_3X_2 layers instead of M_2X layers. Figure 2.4 contains a schematic of these structures. Like mentioned above, these phases are metallic in that they are easily machinable, relatively soft, not susceptible to thermal shock and behave plastically at higher temperature. The Vickers hardness of these phases are mostly in the range of 3-5 GPa, anomalously soft when compared with most other carbides and nitrides. Their thermal and electrical conductivities are excellent and at room temperature fall in the range of 20-40 W/m K, and 1-14 X 10^6 $(\Omega\ m)^{-1}$, respectively. At the same time, they are also ceramic in that they are oxidation-resistant and refractory. These peculiar combinations of machinability, strength and ductility of these compounds can find their origin in their layered structure. The mostly metallic nature of M-X bonds is derived from covalent and ionic contributions. These bonds are exceptionally strong, in contrast with M-A bonds that are relatively weak, especially in shear. [4-15]

Upon pondering over new, plausible host structures in order to find new alternatives for negative electrode material, we realized that there are a number of aspects that make these metallic ceramic phases, $M_{n+1}AX_n$, very attractive in terms of electrochemical storage host structure as well. First of all, based on the compounds invented up to date,

all of the A elements consist of metals that have been known to alloy with lithium to high concentrations. Al, Si, Sn, and Ga are good examples. Since the atomic layer of pure A is chemically very similar to the same metals in bulk or thin film, it seems highly possible that the same elements in atomic layer A should be able to alloy with a high concentration of lithium ions. Also, as depicted in Figure 2.4, A metal layers provide structurally available atomic sites that can store inserted lithium ions. The relatively weaker bonding of A-MX compared to strongly-bonded M-X also generates the chance that the structure can expand normal to the M-X layers in order to accommodate the volumetric expansion of alloying. Furthermore, it seems that the strongly covalent bonds of M-X are unlikely to decompose during lithiation/delithiation, which definitely would help conserve the layered structure and support reversible cycling. Besides, as already mentioned above, these phases are also good electrical conductors, which means that, when we use these phase materials as electrodes, the amount of additives for the purpose of improving conductivity can be reduced or eliminated and also electrode impedance can be lowered.

Based on these favorable features, we could imagine that these compounds might possibly take lithium as intercalating metal through the following alloying reaction.

$$M_{n+1}AX_n + yLi = M_{n+1}ALi_yX_n \qquad \text{[Equation 2.1]}$$

In this assumption, lithium would be inserted or alloyed with the A metallic layers in nanolaminate structure $M_{n+1}AX_n$. We envision that the metallic layer A would react with lithium while M-X layers stay inactive electrochemically upon lithiation/delithiation, supporting reversible alloying. Table 2.2 lists the summary of all $M_{n+1}AX_n$ phases known to date. [4] Among all these phases, compounds of formula M_2AX seem to be

especially attractive candidates for electrode materials, since they possess higher fraction of A relative to M and X and therefore provide larger theoretical gravimetric capacity, when compared to M_3AX_2 and M_4AX_3. Table 2.3 demonstrates gravimetric and volumetric capacity values of several compounds where experimental values [4] of crystal density are available. Here, y represents the number of Li ions inserted into the

Table 2.2 Summary of all $M_{n+1}AX_n$ compounds known to date.

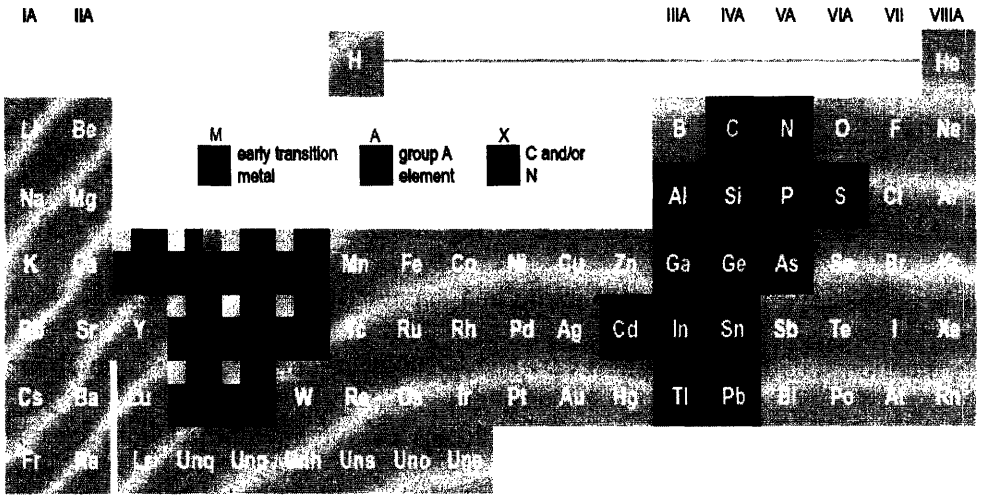

211					
Ti_2AlC^*	Ti_2AlN^*	Hf_2PbC^*	Cr_2GaC	V_2AsC	Ti_2InN
Nb_2AlC^*	$(Nb,Ti)_2AlC^*$	$Ti_2AlN_{0.5}C_{0.5}^*$	Nb_2GaC	Nb_2AsC	Zr_2InN
Ti_2GeC^*	Cr_2AlC	Zr_2SC	Mo_2GaC	Ti_2CdC	Hf_2InN
Zr_2SnC^*	Ta_2AlC	Ti_2SC	Ta_2GaC^*	Sc_2InC	Hf_2SnN
Hf_2SnC^*	V_2AlC	Nb_2SC	Ti_2GaN	Ti_2InC	Ti_2TlC
Ti_2SnC^*	V_2PC	Hf_2SC	Cr_2GaN	Zr_2InC	Zr_2TlC
Nb_2SnC^*	Nb_2PC	Ti_2GaC	V_2GaN	Nb_2InC	Hf_2TlC
Zr_2PbC^*	Ti_2PbC^*	V_2GaC	V_2GeC	Hf_2InC	Zr_2TlN

312		413	$Ti_4AlN_3^*$

Table 2.3 Theoretical capacities of several H-phase materials

Material	Form. Wt. (g/mole)	Density (g/cm^3) [4]	Capacity, y=1, mAh/g (Ah/L)	Capacity y=2	Capacity y=3	Capacity y=4
Ti_2AlC	134.75	4.11	198.9(817.6)	397.9(1635.0)	596.8(2452.8)	795.7(3270.4)
Ti_2AlN	136.75	4.31	196.0(844.8)	392.0(1689.7)	588.1(2534.5)	784.1(3379.4)
V_2AlC	140.87	4.07	190.3(774.5)	380.6(1548.9)	570.9(2323.4)	761.2(3097.9)
Ti_2SC	139.84	4.62	191.7(885.6)	383.4(1772.2)	575.1(2656.8)	766.8(3542.4)
Ti_2SnC	226.48	6.36	118.4(752.8)	236.7(1505.5)	355.1(2258.1)	473.4(3010.8)
Ti_3SiC_2	195.75	4.52	136.9(618.8)	273.9(1237.9)	410.7(1856.4)	547.6(2475.2)
Cr_2GaN	187.72	6.82	142.8(973.9)	285.6(1947.8)	428.4(2921.7)	571.2(3895.6)

structure per unit cell. Compared to the gravimetric capacity, 372 mAh/g, and the volumetric capacity, 836.9 Ah/L), of graphite [16, 17], gravimetric capacity values of these compounds especially for y greater than about 2 and volumetric capacity values for y values greater than about 1 seem fairly advantageous. Moreover, given that the chemical identity of group A element layers is similar to bulk metal, there is also potential advantages at which alloying takes place. The potentials of bulk metal, Sn, Si, and Al are known to be less than 0.5V and the potentials of compounds $M_{n+1}AX_n$ are expected to be similar to low like the bulk. This will result in energy density advantages of these compounds over graphite as well.

2.4 Selection of Cr-Ga-N system

Considering various aspects listed in the previous section, $M_{n+1}AX_n$ phases seem quite fascinating as possible electrodes in lithium ion batteries. Among over 50 compounds of $M_{n+1}AX_n$ that have been experimentally synthesized to date (Table 2.2), we chose several promising compounds according to the following criteria. First of all, given that the atomic layer of A in this layered structure are chemically similar to the same metals in bulk or thin films or nanocrystalline form, group A elements that are able to electrochemically accommodate a high concentration of lithium ion are favorable. Al, Si, Sn and Ga correspond to this. Secondly, for early transition metal M, rather than expensive and heavy-weight elements such as Ta, Hf, elements easy to obtain commercially are selected. Ti, V and Cr apply to this based on Table 2.2. Thirdly, compounds of which properties have been relatively well-studied take priority over others. Researchers have examined a number of methods to fabricate a single-phase Ti_3SiC_2 and its properties and the amount of study on Ti_3SiC_2 [4-6, 10, 13, 14, 18] is tremendous compared to other same kind of compounds. Lastly, as mentioned previously, 211 phases are more advantageous than 312 and 413 phases, since the former ones would have a high relative fraction of A relative to M and X, and therefore a high theoretical capacity. According to these criteria, Ti_2AlC, Ti_2SnC, Ti_2AlN, Cr_2GaN, Ti_3SiC_2 and Ti_3AlC_2 are singled out.

We decided to try Cr_2GaN, a layered ternary nitride in order to see if and how this compound would react with lithium electrochemically. Like the other 211's, the structure of Cr_2GaN, consisting of Cr-N layers interleaved with layers of pure Ga, is hexagonal with lattice parameter *a* and *c* of 2.88 and 12.7 Å, respectively. [19] In Cr_2GaN, self-extrusion of Ga whisker at room temperature is observed by M.W.

Barsoum et al. In their work [12], filaments of pure elemental gallium is observed to extrude from bulk Cr_2GaN at room temperature in air and the author of this work describes this phenomenon as a room-temperature deintercalation of gallium from the basal plane of porous Cr_2GaN samples, based on their XRD patterns and SEM pictures. The XRD and SEM pictures are illustrated in Figure 2.5 and Figure 2.6, respectively. The fact that the A atom Ga is able to extrude from CrN layers as metallic Ga seems to support the reversible alloying mechanism that we assumed previously for $M_{n+1}AX_n$ family materials as electrodes for batteries. This self-extrusion phenomenon implies not only that A layers do behave as essentially metallic but also that extrusion could be another mechanism by which the strain can be accommodated upon alloying that causes volumetric expansion of the A layers. Theoretically, Cr_2GaN could show 285.6 mAh/g and 1947.8 Ah/L for gravimetric capacity value and volumetric capacity value,

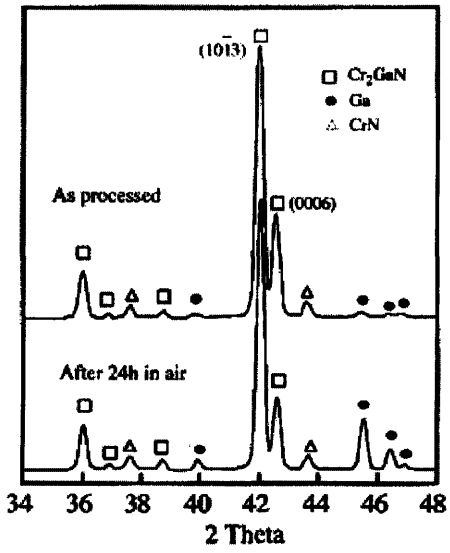

Fig. 2.5 XRD of as-processed samples of Cr_2GaN and the same surface after exposure to the atmosphere for 24 hours at room temperature. Note emergence of Ga peaks and reduction in the peak intensities of the basal, or (0006) planes of Cr_2GaN. [12]

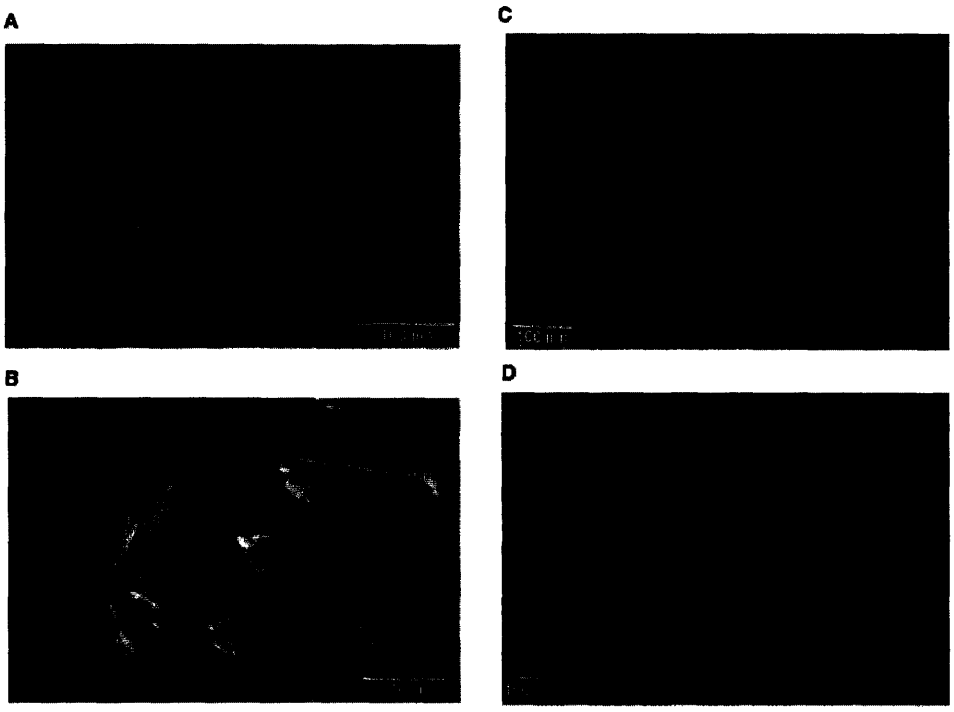

Fig. 2.6 A series of SEM images of the surface of a Cr2GaN sample exposed to the atmosphere for 50 hrs. A) Filaments observed are pure single crystal-line Ga. B) Same as (A), but at higher magnification. C) Same as A), but at a different location, D) the sample after six months, showing marked increase in density and lengths of whiskers [12]

respectively, provided that Cr_2GaN adopt two lithium atoms per one atomic unit. (Table 2.4) These values are quite comparable to those of graphite. (372 mAh/g and 837 Ah/L for gravimetric capacity and volumetric capacity, respectively). Investigating the synthesis and electrochemical performance of Cr_2GaN is meaningful in that this could be the groundwork for a totally new class of energy storage materials if Cr_2GaN turns out to be electrochemically active. Furthermore, it is a good opportunity to analyze the mechanism of Li-Ga reaction, since the basic idea is use gallium metal layer as an active material in a form of new structure, M_2AX.

From a perspective of synthesis, the fabrication of pure single-phase Cr_2GaN as well as

all other H-phases is still an issue. We also obtained several samples composed of several Cr-Ga-N phases [20, 21] such as Ga, Cr-N phases, GaN, Cr-Ga phases and Cr_3GaN. Some are formed during synthesis and the others are from starting materials remaining unreacted. Accordingly, in order to study the electrochemical performances of Cr_2GaN and deduce the correspondent reaction mechanism, it is necessary to understand the synthesis and electrochemical properties of Cr-Ga-N systems as well. Detailed phases of interest in the Cr-Ga-N system will be treated in Chapter 3.

2.5 Difficulties in this research

In this last section of Chapter 2, several obstacles that prevent from stepping forward to this research are described.

Like mentioned previously, in a family compound of general formula, $M_{n+1}AX_n$, synthesizing a single phase sample is also a significant issue. For Cr_2GaN as well, it is hard to acquire a sample of a single-phase because Cr_2GaN is thermodynamically stable with other Cr-Ga-N phases depending on firing temperature and hours. For example, GaN is known to coexist with Cr_2GaN at 740 ℃.[21]

Secondly, the existence of group A element such as Ga and Sn in the sample is also problematic. As elemental gallium also reacts with lithium electrochemically, when gallium exists in the sample, it is difficult to tell the difference between the electrochemical properties from elemental gallium and those from Cr_2GaN and other compounds. Worse situation is that this elemental gallium is not identified in XRD due

to amorphous characteristic although quite an amount of it still stays in the sample. This will be shown in Chapter 3. Therefore, elimination of residue of group A element is very necessary but not easy.

Moreover, in order to avoid oxidation from air, complex synthesis procedure is required. Despite this, during electrochemical testing preparation, there is still possibility of oxidation or moisture absorption in samples. When oxidized, samples sometimes include oxides with which Li-driven electrochemical reaction occurs.

2.6 References

1. [cited; Available from: http://en.wikipedia.org/wiki/Gallium.
2. Limthongkul, P., *Phase transformations and microstructural design of lithiated metal anodes for lithium-ion rechargeable batteries*, in *Dept. of Materials Science and Engineering*. 2002, Massachusetts Institute of Technology, Cambridge.
3. Saint, J., et al., *Exploring the Li-Ga room temperature phase diagram and the electrochemical performances of the LixGay alloys vs. Li.* Solid State Ionics, 2005. **176**(1-2): p. 189-197.
4. Barsoum, M.W., *The MN+1AXN phases: A new class of solids : Thermodynamically stable nanolaminates.* Progress in Solid State Chemistry, 2000. **28**(1-4): p. 201-281.
5. Barsoum, M.W., D. Brodkin, and T. El-Raghy, *Layered machinable ceramics for high temperature applications.* Scripta Materialia, 1997. **36**(5): p. 535-541.
6. Barsoum, M.W. and T. El-Raghy, *Room-Temperature Ductile Carbides.* Metallurgical and Materials Transactions A, 1999. **30A**: p. 363-369.
7. Barsoum, M., T. El-Raghy, and M. Ali, *Processing and characterization of Ti2AlC, Ti2AlN, and Ti2AlC0.5N0.5.* Metallurgical and Materials Transactions A, 2000. **31**(7): p. 1857-1865.
8. Barsoum, M., T. El-Raghy, and A. Procopio, *Synthesis of Ti4AlN3 and phase equilibria in the Ti-Al-N system.* Metallurgical and Materials Transactions A, 2000. **31**(2): p. 373-378.
9. Barsoum, M., T. El-Raghy, and A. Procopio, *Characterization of Ti4AlN3.*

Metallurgical and Materials Transactions A, 2000. **31**(2): p. 333-337.

10. Barsoum, M.W., et al., *Thermal properties of Ti3SiC2.* Journal of Physics and Chemistry of Solids, 1999. **60**(4): p. 429-439.
11. Barsoum, M.W., G. Yaroschuk, and S. Tyagi, *Fabrication and characterization of M2SnC (M=Ti, Zr, Hf and Nb).* Scripta Materialia, 1997. **37**: p. 1583-1591.
12. Barsoum, M.W. and L. Farber, *Room-Temperature Deintercalation and Self-Extrusion of Ga from Cr2GaN.* Science, 1999. **284**(5416): p. 937-939.
13. El-Raghy, T. and M.W. Barsoum, *Processing and Mechanical Properties of Ti3SiC2: I, Reaction Path and Microstructure Evolution.* J. Am. Ceram. Soc., 1999. **82**(10): p. 2849-2854.
14. El-Raghy, T., et al., *Processing and Mechanical Properties of Ti3SiC2: II, Effect of Grain Size and Deformation Temperature.* J. Am. Ceram. Soc., 1999. **82**(10): p. 2855-2860.
15. El-Raghy, T., S. Chakraborty, and M.W. Barsoum, *Synthesis and characterization of Hf2PbC, Zr2PbC and M2SnC (M=Ti, Hf, Nb or Zr).* Journal of the European Ceramic Society, 2000. **20**(14-15): p. 2619-2625.
16. Dahn, J.R., *Carbon and graphites as substitutes for the lithium anode.* Industrial Chemistry Library, 1994. **5**.
17. Mohri, M., *Rechargeable lithium battery based on pyrolytic carbon as a negative electrode.* J. Power Sources, 1989. **26**: p. 545-551.
18. El-Raghy, S.M., et al., *Preliminary Report on the Electrochemical Behavior of Ti3SiC2.* Journal of Materials Science Letters, 1999. **18**(7): p. 519-520.
19. Beckmann, O., et al., Monatsh. Chem., 1969. **100**: p. 1465.
20. Mohney, S.E., D.J. MacMahon, and K.A. Whitmire, *Condensed phase equilibria*

in the Cr-Ga-N system. Materials Science and Engineering B, 1997. **49**(2): p. 152-154.

21. Farber, L. and M.W. Barsoum, *Isothermal sections in the Cr–Ga–N system in the 650–1000 °C temperature range.* J. Mater. Res., 1999. **14**: p. 2560-2566.

3. Chapter 3 Synthesis and structure of Cr-Ga-N system

3.1 Starting materials

In order to obtain Cr_2GaN, we used i) Ga pellets and Cr_2N powder and ii) GaN powder and Cr powder as the starting materials. For convenience, depending on which combination of starting materials was used, we denoted the samples produced from Ga shots and Cr_2N as GaEx # (#: sample number) and designated the samples from the mixture of GaN and Cr as CGN#. Although there are detailed differences in each synthesis step among product samples, basically, all the samples of GaEx's and CGN's were synthesized through the following five steps: weighing, mixing, iso-pressing, vacuum-sealing and heat treatment. Detailed procedures will be explained in the following sections.

3.2 GaEx samples

3.2.1 Experimental procedures

Gallium pellets (6mm diameter; Alfa Aesar, 99.9999% purity, metals basis) and Cr_2N (-325 mesh; GFS chemicals) were weighed to correspond to the 211 chemistry or other stoichiometric value in the vicinity of 211 chemistry. In order to attain homogeneity as much as possible, gallium pellets were cut into pieces by razor blade before hand-mixing so that more gallium metal surface could be exposed to and evenly mixed with chromium nitride powder as much as possible. After hand-mixing, mixture of gallium

pellets and chromium nitride were put into the "finger" from a latex glove. This "finger" bag was tied and then put into the plastic tubing. Plastic tubing helped the mixture lump maintain a certain shape inside latex. All the procedures up to this were conducted under argon atmosphere in order to avoid oxidation. This tightly sealed sample was taken out of argon chamber and then put into another plastic bag. The air inside of this bag finally was evacuated by vacuum pump and thermally sealed. This step is necessary to prevent the oil from leaking into the sample during isostatic pressing. Thoroughly sealed samples were cold isostatically pressed until the pressure reached 42000 psi and then held at that pressure for 3 minutes. When all starting materials were in powder type, through this procedure, a single dense piece that was ~4 cm long, ~4-5 mm diameter was usually produced through when removed from all surrounding bags. However, from the mixture of gallium pellets and chromium powder, due to the characteristics of the form of gallium, the best specimen that could be obtained after cold isostatic pressing was in the form of gallium pellets of which surface is covered by chromium powder as much as possible. This was one of the reasons why GaN and Cr, both existing in powder form were tried later so that much more evenly mixed sample could be generated. As shown later, these powder-type starting materials allowed mixing by milling tools and this contributed a lot to homogeneity of the resulting specimens. Back to the procedure, after isostatic pressurizing step, the specimen prepared above was put into a fused quartz tube and vacuum-sealed. Although the time to take for vacuuming varied according to the condition of sample pieces, the vacuuming step usually took around 24 hours for our samples. This vacuum sealing procedure was carried out by help of Yinlin Xie, a technical staff member at MIT. In order to minimize exposure time to air, it was recommended to take the pressurized sample out of the enclosing plastic bags and

tubing used in the previous steps right before the encapsulation step began. This encapsulated quartz tube containing green body was finally placed in the middle of quartz tube furnace and fired at the desired temperature. In order to find the optimum processing temperature for Cr_2GaN, various conditions (firing temperatures and times) were chosen and tried out. Referring to previously published studies on Cr-Ga-N system materials [1, 2], we considered that the optimum processing temperature range for Cr_2GaN is 650-800 ℃. According to L. Farber and M.W. Barsoum [2], above 910 ℃, Cr_2GaN becomes unstable and decomposes, and below 650 ℃ the reaction kinetics are quite sluggish. They also reported in another literature [3] that they obtained Cr_2GaN with minor amounts of other phase materials through HIPing and annealing the mixture of gallium metal and CrN + Cr_2N at 740 ℃ for 24 hours. Therefore, in our work, we set the annealing temperatures and times with some variation, based on these reports mentioned above. Eight individual runs were conducted with different conditions (temperatures, times and compositions) and summarized in Table 3.1. As demonstrated in Table 3.1, several runs included two or more steps of heat treatment. As reported in reference [2], in M.W. Barsoum group's way, the pellet specimens were again hot isostatically pressed at 850 ℃ for 8 hours after being cold pressed. Hot isostatic pressing (HIP) played a role in restraining the expansion of samples while temperature increased. In our preliminary work, it was observed that the volume of our sample expanded little during firing without simultaneous pressurizing. Accordingly, in order to save time and expense, we decided to skip hot isostatic pressing step in our work unlike M.W. Barsoum group's experimental method. In GaEx 1, 2 and 3, the first step heat treatment conditions were varied while all other parameters including secondly annealing temperatures and times were set the same as 740 ℃ and for 24hrs. In GaEx 4,

after ramping up to 850 ℃, the specimen was controlled to directly reach 740 ℃ and annealed without going through cooling to room temperature between steps. In GaEx 5, only one step heat treatment, that is, annealing at 740 ℃ for 24 hrs was run. From GaEx1 to GaEx 5, the atomic composition ratio of gallium and Cr_2N was 1.7 : 1 by accident. This was not done intentionally in the beginning but later it turned out that results from gallium excess samples were greatly useful to analyze overall Cr-GaN system of our interest. As our goal was to attain Cr_2GaN, specimens composed of 1:1 atomic ratio of gallium and Cr_2N were prepared again and fired at various conditions as shown in GaEx 6-8 in Table 3.1 In all runs, the heating rate was 10 ℃/minute. After heat treatments, the samples were removed from the quartz tube and then crushed in a mortar and pestle. Part of the resulting powder was used for phase identification while the remainder was saved for electrochemical characterization. Phase identification was performed using Rigaku Powder Diffractometers.

3.2.2 Results and Discussion

X-ray diffraction (XRD) of the final compounds from eight individual runs indicated that all resulting powders from GaEx samples included Cr_2GaN, Cr_3GaN (or $Cr_3GaN_{0.5}$) as main compounds in phase identification. In this work, XRD patterns were analyzed using MDI JADE 5.0 program. Although there are many other parameters that should be considered to determine the relative amount of individual compounds in each sample accurately, it is useful to compare relative peak intensity heights of identified phases in order to see qualitatively the relative amounts of resulting phases in the final samples. Considering relative intensity peak height of XRD spectrums (Figure 3.1, Figure 3.2,

Table 3.1 Summary of compositions, times and temperatures of runs carried out on GaEx samples

Sample	Composition (molar ratio of Ga : Cr_2N)	Heat treatment profile
GaEx 1	1.7 : 1	850 ℃ 8hrs ⇨ RT ⇨ 740 ℃ 24hrs ⇨ air quenching
GaEx 2	1.7 : 1	850 ℃ 8hrs ⇨ RT ⇒1000 ℃ 4hrs ⇨ RT ⇒ 740 ℃ 24hrs ⇨ Air quenching
GaEx 3	1: 1	900 ℃ 8hrs ⇨ RT ⇨ 740 ℃ 24hrs ⇨ Air quenching
GaEx 4	1.7 : 1	850 ℃ 8hrs ⇨ 740 24hrs ⇨ Air quenching
GaEx 5	1.7 : 1	740 ℃ 24hrs ⇨ Air quenching
GaEx 6	1:1	740 ℃ 24hrs ⇨ air quenching
GaEx 7	1:1	740 ℃ 18hrs ⇨ Air quenching
GaEx 8	1:1	740 ℃ 48hrs ⇨ Air quenching

Figure 3.3), it was observed that more Cr_2GaN was created than Cr_3GaN in all GaEx samples from the mixture of gallium metal and chromium nitride powder. The formation of Cr_3GaN requires more Cr atoms than that of Cr_2GaN. As our GaEx samples contained requisite amount of gallium or excess gallium for stoichiometric Cr_2GaN, chromium elements in our starting material mixture seemed to be in short supply for Cr_3GaN formation. Also, while creation of Cr_2GaN demands combination of Cr_2N and Ga only, formation of Cr_3GaN seems to necessitate bond breakage between Cr-N of Cr_2N in order to provide 3 Cr atoms per 1 Ga atom and 1 N atom from the mixture of Cr_2N and Ga. Thus, for these reasons, it was thought that synthesis of Cr_2GaN took place more favorably than the creation of Cr_3GaN from our GaEx samples. Besides, it drew our attention that no trace of crystalline gallium appeared in the XRD pattern of GaEx 2 as illustrated in Figure 3.1. Since the amount of gallium metal was put in excess compared to the amount of chromium nitride in GaEx 1-5, it logically follows that quite an amount of gallium should remain in the final samples after Cr_2GaN and Cr_3GaN were produced. This owes to the fact that gallium metal is near its amorphous liquid state near room temperature. Crystalline gallium peaks were observed in the XRD patterns of a few samples such as GaEx1 and GaEx3 (Figure 3.2). Yet, the intensity of these crystalline gallium peaks was weaker than those of Cr_2GaN and Cr_3GaN. As more details will be explained in chapter 4, at least around 45 % of the total composition of GaEx samples (GaEx 1- GaEx 5) was supposed to comprise gallium metal either in crystalline or amorphous form. This is deduced from comparison of the electrochemical capacity value. Then, if all 45 % of the total sample weight of gallium metal had been in crystalline form, the peak intensity of gallium phase should have been much higher than those of C_2GaN and Cr_3GaN in the XRD patterns of GaEx1 and

GaEx3. This tells us that amorphous gallium metal that wasn't detected in XRD still existed even in the samples where crystalline gallium phase appeared in the XRD patterns. Even for GaEx 6-8 of which starting materials corresponded to 211 chemistry, it was verified that quite an amount of gallium still remain in these samples although no peaks of crystalline gallium emerged in the XRD patterns. More detail on how this was verified will be treated in chapter 4 again. It is surprising that such an amount of gallium metal cannot be detected in XRD. Also, there were some unknown minor peaks in these GaEx XRD patterns. These peaks were not in correspondance to those of any compound that could be formed from elements Cr, Ga, and N, at least in phase identification of MDI JADE program. Since the peaks of $Cr_3GaN_{0.5}$ and Cr_3GaN are overlapped, those two phases were indicated without thorough distinction in our figures.

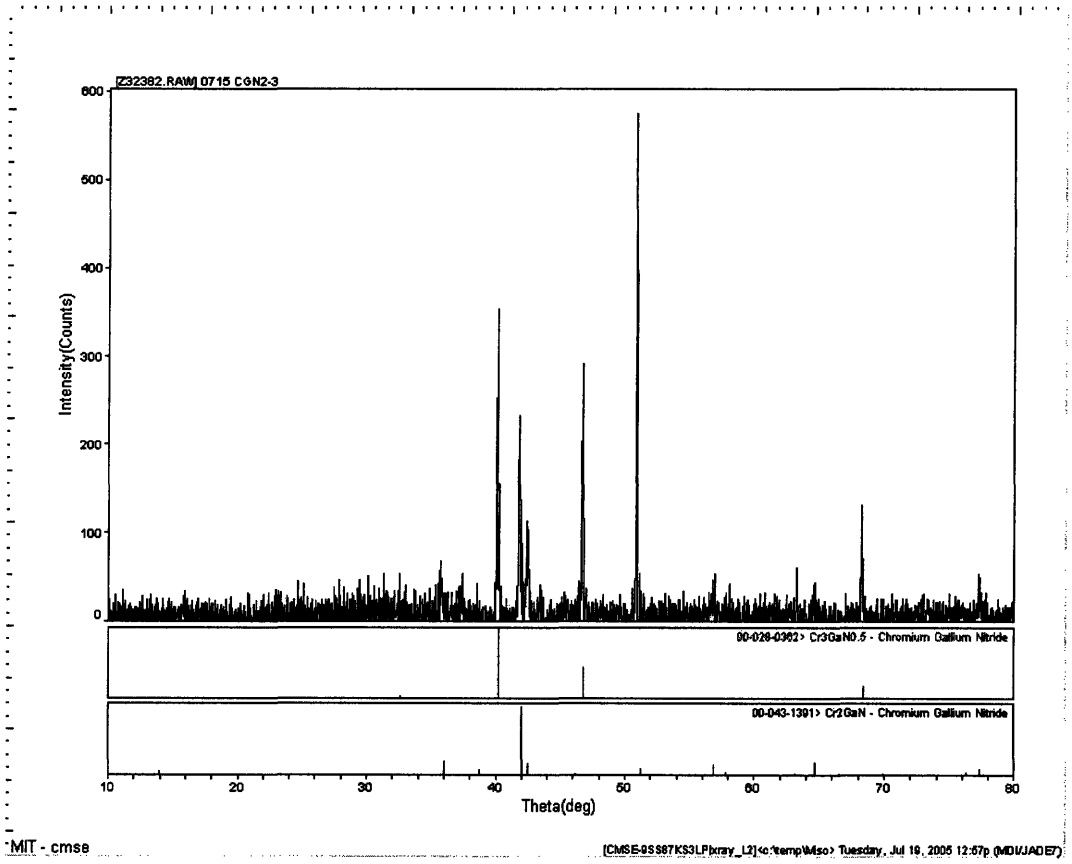

Fig. 3.1 XRD patterns of GaEx 2 sample

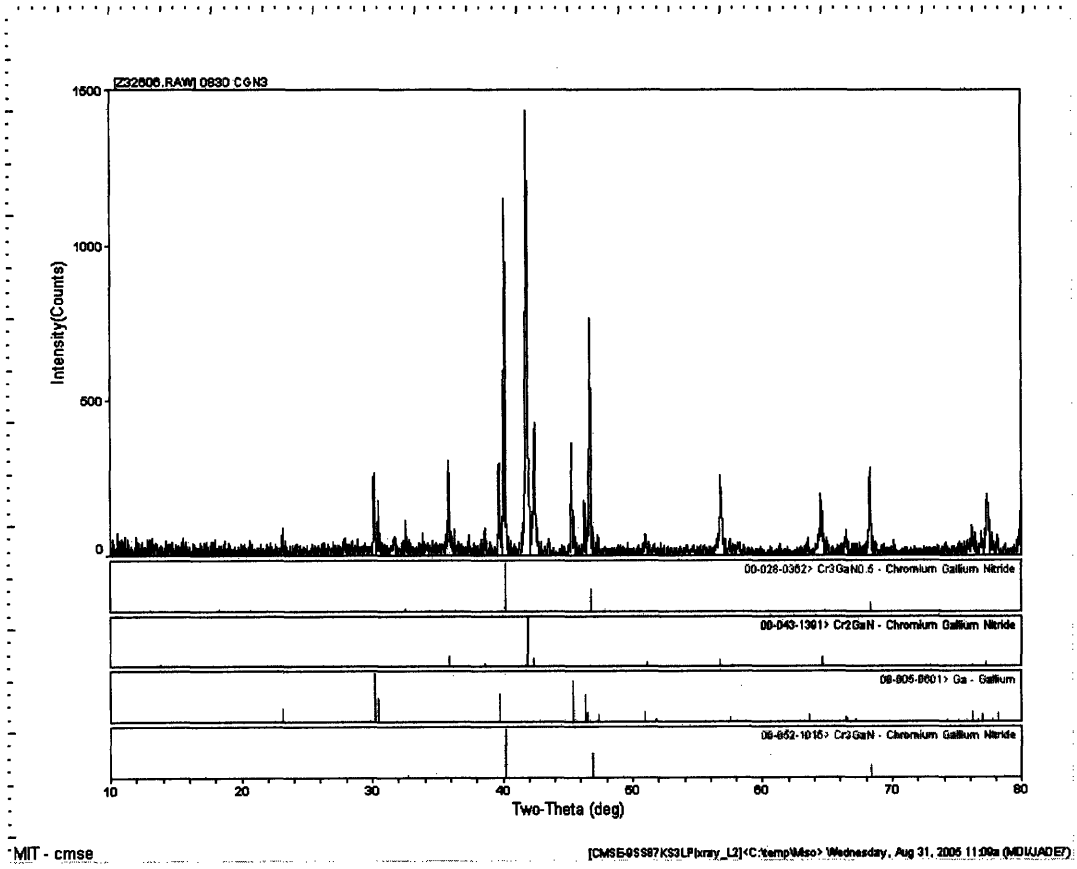

Fig. 3.2 XRD patterns of GaEx 3 sample

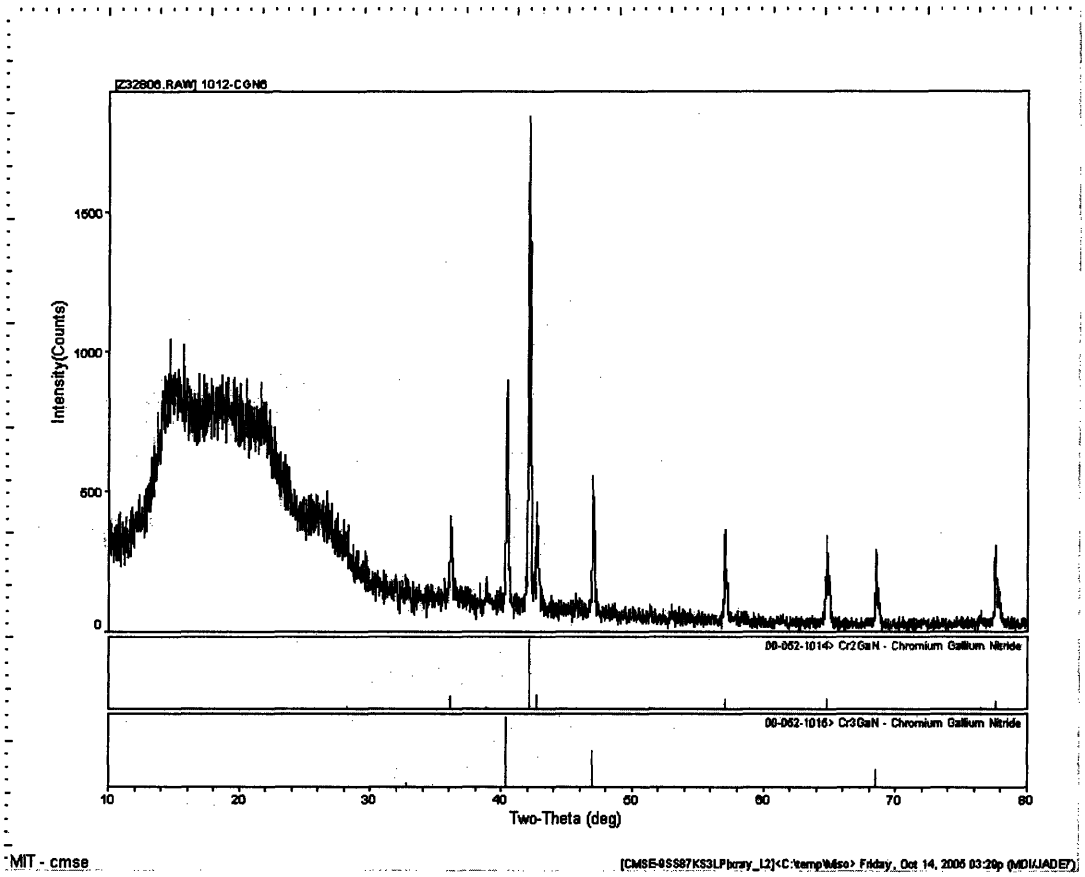

Fig. 3.3 XRD patterns of GaEx 6 sample

3.3 CGN samples

As previously shown, when gallium metal and chromium nitride (Cr_2N) were used as starting materials to produce Cr_2GaN, it was very hard not only to detect but also to eliminate gallium metal in the final samples. This prevented us from fabricating the desired compound and testing electrochemical performance of Cr_2GaN or other phases in Cr-Ga-N system. Furthermore, the coarse pellet-type form of raw gallium metal restricted homogeneous mixing of starting materials during synthesis. Hence, we chose to start with GaN and Cr, both commercially available in powder type. This way allows mixing step by use of milling tools during fabrication so that the homogeneity of mixture of starting materials could be increased. Moreover, the possibility that gallium metal would exist in the resulting powders could be greatly lowered so that electrochemical characterization of Cr-Ga-N system could be investigated under little effect of gallium metal. Final products from starting powders GaN and Cr are denoted as CGN# (# : number) in order to differentiate from the previously synthesized GaEx samples.

3.3.1 Experimental procedures

CGN samples were fabricated by similar way to the synthesis of GaEx samples: weighing, mixing by using milling facilities, cold isostatic pressing, vacuum-sealing, and heat treatment. Gallium nitride (-325 mesh; Alfa Aesar, 99.99 % purity, metals basis) and chromium powder (-100+325 mesh; Alfa Aesar, 99.99 % purity) were weighed and dry mixed in an alumina milling jar to yield the Cr_2GaN stoichiometry. O-

ring was used to seal the alumina jar in the argon-filled glove box in order to minimize exposure to air. Sealed jar was put on roller mill and spun at 300 rpm for 24 hours for mixing purpose. The mixture was cold iso-pressed at 42000 psi for 3 minute into a single dense yellowish dark gray piece that is ~4 cm long and ~4-5 mm diameter. (The color of GaN powder is light yellow and the color of Cr is dark gray.) Like GaEx sample preparation, latex "finger" from glove, plastic tubing and plastic bags were used to cover and seal the mixture in turn before isostatic pressing and peeled off right before the next step (vacuum sealing). The specimens were encapsulated in quartz tube into vacuum atmosphere before annealing. Heat treatment was conducted in a quartz tube furnace with ramping rate, 10℃/minute. As in GaEx's synthesis, we employed several heat treatment conditions for CGN samples that were listed in Table 3.2. After each sample fabrication, XRD was run on the resulting CGN powders for phase identification. We focused mainly on obtaining the samples that contained as much amount of ternary Cr-Ga-N compounds such as Cr_2GaN and Cr_3GaN as possible for our future characterization.

3.3.2 Results and Discussion

XRD patterns of several CGN samples are demonstrated from Figure 3.4 through Figure 3.8. Depending on samples from individual heat treatment experiment sets, relative amount of Cr_2GaN, Cr_3GaN, GaN, Cr and oxides differed. GaN and Cr were regarded to remain unreacted from starting mixture due to the fact that factors such as temperatures and times were not sufficiently met. CGN4 was synthesized by firing stoichiometric mixture at 740 ℃ for 9 hours. Relatively high intensity peaks of GaN in the XRD

Table 3.2 Summary of heat treatment conditions for CGN samples

Sample	Heat treatment profile (all followed by air-quenching)	Specifics
CGN 1	850 ℃ 8hrs ⇨ 740 ℃ 24 hrs	
CGN 3	740 ℃ 18hrs	Pressed at 18000 psi
CGN 4	740 ℃ 9hrs	
CGN 5	850 ℃ 8hrs ⇨ 740 ℃ 24hrs	Mixture corresponding to 311 chemistry
CGN 6	740 ℃ 18hrs	
CGN 7	740 ℃ 100 hrs	
CGN 9	800 ℃ 24 hrs	

patterns of CGN4 (Figure 3.4) indicated that quite an amount of GaN wasn't able to react due to lack of reacting time. In case of the samples (CGN6 and CGN7) annealed at the same temperature for longer hours (Figure 3.6 and Figure 3.7) compared to CGN4, GaN phase was not distinctly identified in the XRD patterns. Sample CGN3 also was found to contain an appreciable amount of GaN. Compared to CGN6, CGN3 was differently produced in that the stoichiometric mixture was pressed at lower pressure (18000 psi) during cold isostatic pressing step. (Normally, samples were pressed at 42000 psi.) Pressing at relatively lower pressure seemed to affect the extent of density of the sample. In a less compact mixture sample, the distance among powders would be longer and thus reaction among powder materials would take place less actively compared to the reaction in a denser mixture piece. As illustrated in Figure 3.6 and Figure 3.7, CGN6 and CGN7 that were annealed at 740 ℃ for 18hrs and 100hrs, respectively, were mainly composed of Cr_2GaN and Cr_3GaN. Comparison of the relative peak intensities in the XRD patterns of CGN6 and CGN7 (Figure 3.6 and Figure 3.7, respectively) tells us firstly that too many hours of annealing at that temperature cause Cr_2GaN to decompose and secondly, Cr_3GaN stays more stable when fired at 740 ℃ for longer time than Cr_2GaN. In an attempt to yield a single phase of Cr_3GaN, sample CGN5 was synthesized by weighing the requisite amount of GaN and Cr, following the same procedures as other samples and heat treated as listed in Table 3.2. Provided that undetectable amorphous phases by XRD didn't exist, almost a single phase of Cr_3GaN was formed and identified by XRD in CGN5. The broad peak looking like a hump at lower degrees in the XRD pattern of CGN5 (Figure 3.5) gave us doubt whether any amorphous phases were formed. This will be mentioned again in more detail later in chapter 4. The result that single phase of Cr_3GaN was more easily

produced at 740 ℃ than Cr_2GaN from GaN and Cr mixture suggested that equilibrium state of Cr_3GaN could be reached much faster than that of Cr_2GaN at 740 ℃ from this mixture. For CGN9, based on our previous experimental results, we decided to try annealing for 24 hours at a temperature that is higher than 740 ℃ but should be lower than 850 ℃ (decomposition temperature of Cr_2GaN). From this attempt, sample CGN9 that seemed to contain more amount of Cr_2GaN than Cr_3GaN was obtained. Peaks of Cr_2O_3 also appeared in the XRD patterns of CGN9 (Figure 3.8) and this seemed to attribute to the oxidation of starting element Cr powder during fabrication procedures. From the analysis of CGN9, 800 ℃ seemed to be a better optimum temperature to synthesize Cr2GaN than 740 ℃. All the analysis above was established upon the assumption that there were no other major phases that were not detectable in XRD like the case of amorphous gallium metal in GaEx samples. Observation that at least no crystalline gallium phase was identified in XRD patterns confirmed that the possibility that pure gallium exists was lower in CGN's than in GaEx's.

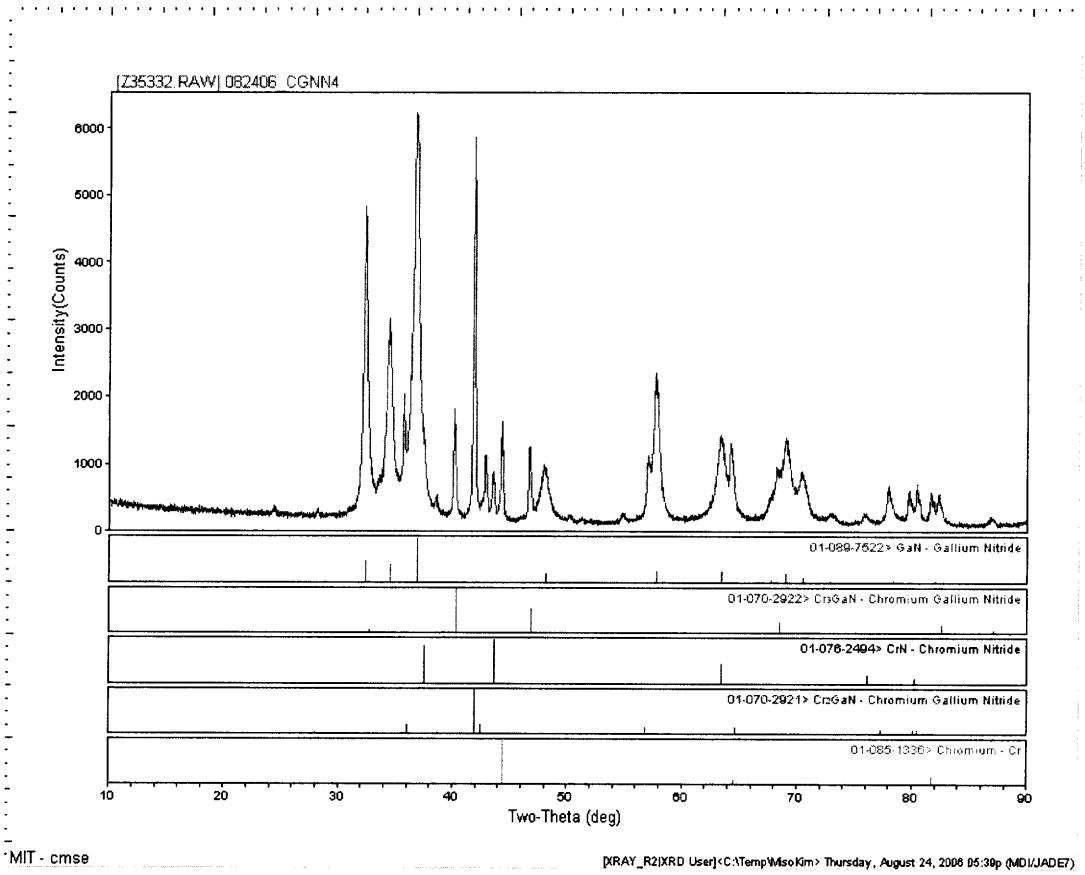

Fig. 3.4 XRD patterns of CGN 4 sample

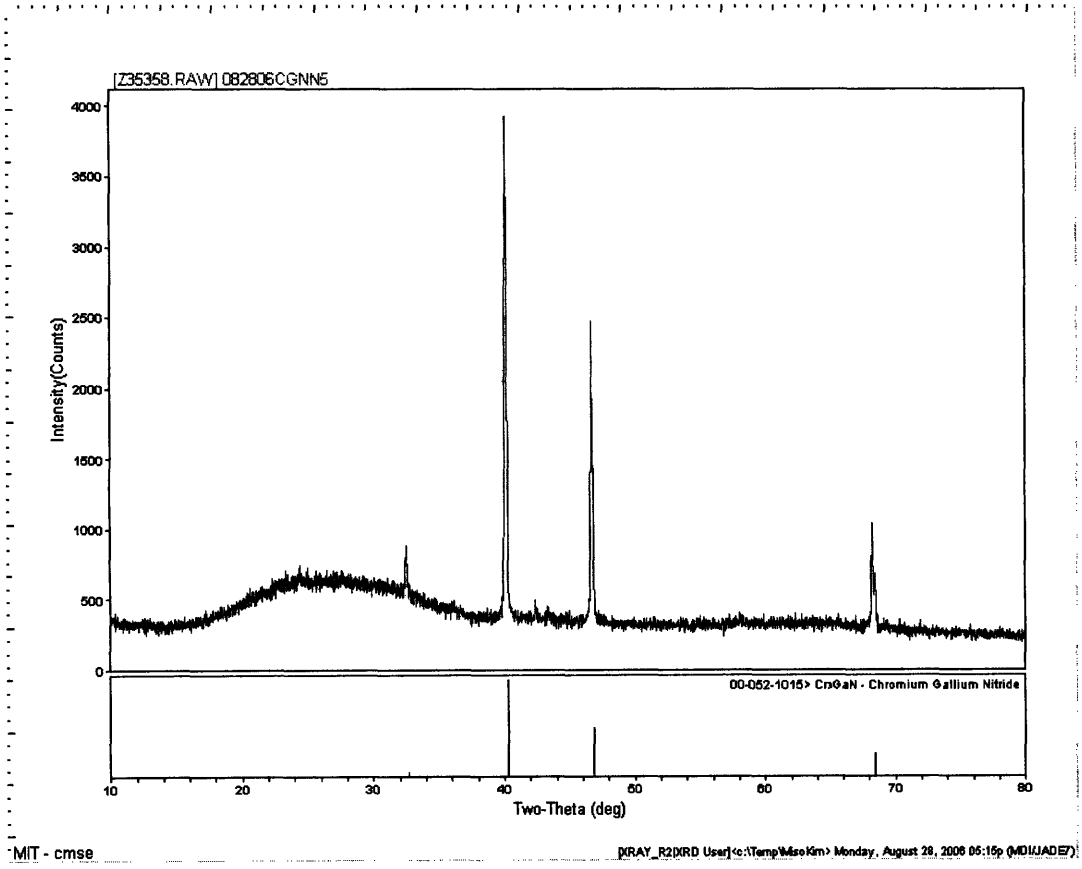

Fig. 3.5 XRD patterns of CGN 5 sample

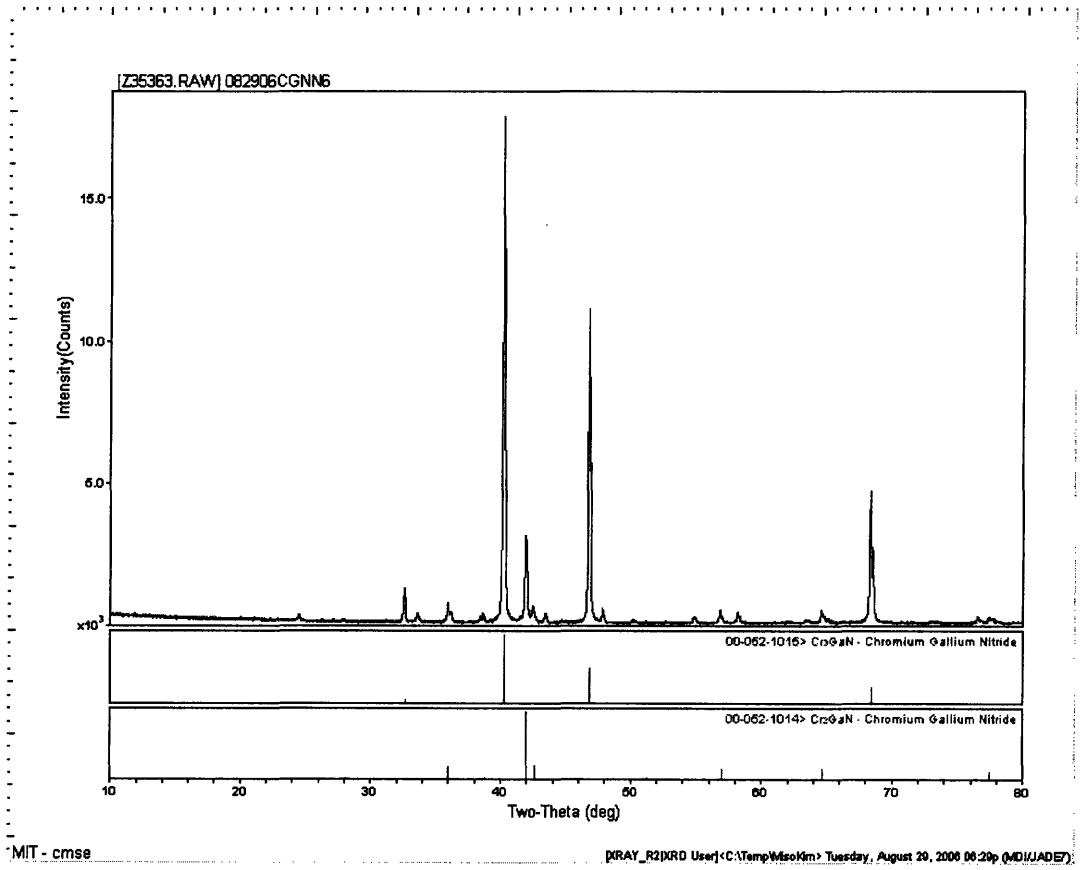

Fig. 3.6 XRD patterns of CGN 6 sample

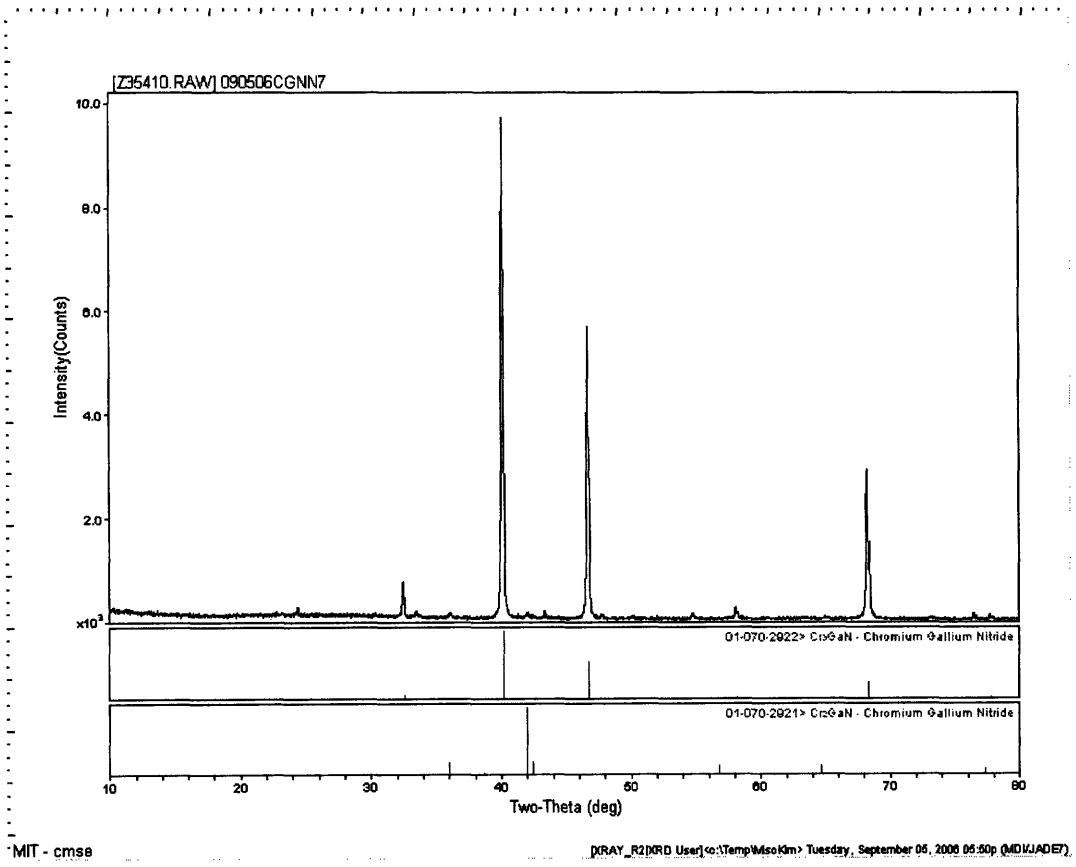

Fig. 3.7 XRD patterns of CGN 7 sample

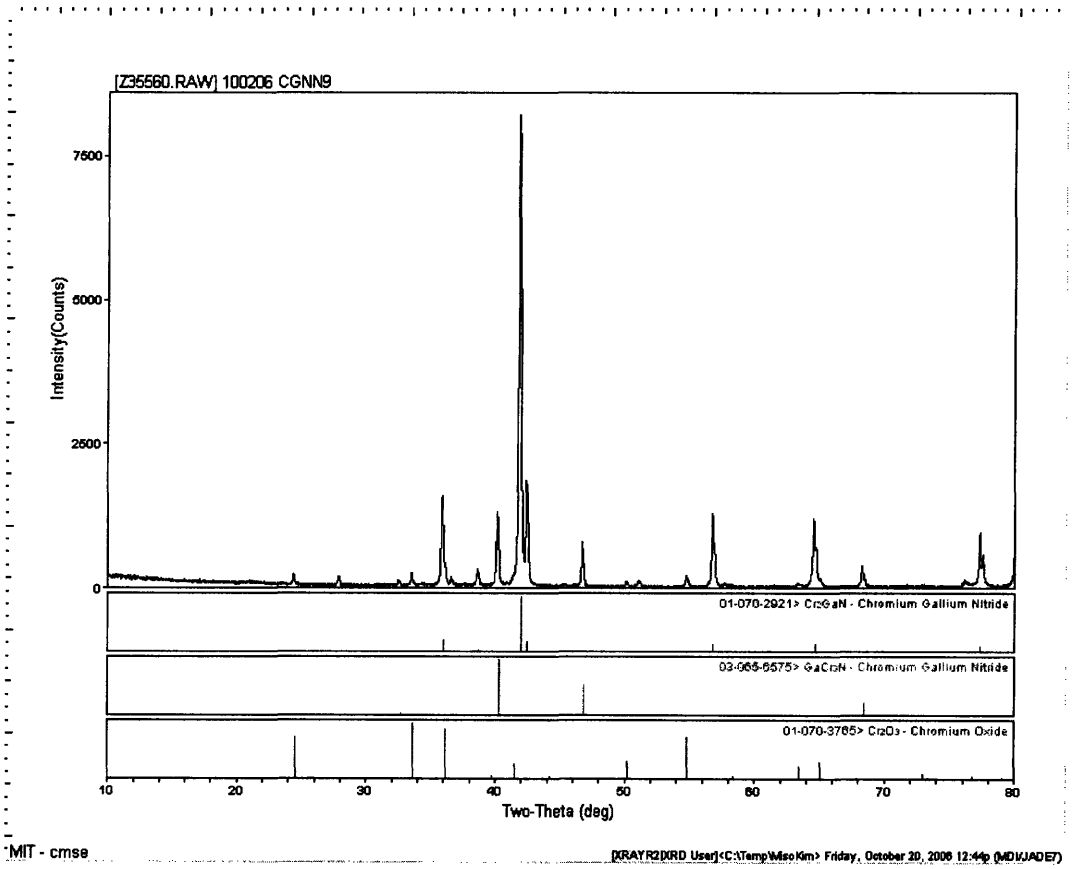

Fig. 3.8 XRD patterns of CGN 9 sample

3.4 References

1. Mohney, S.E., D.J. MacMahon, and K.A. Whitmire, *Condensed phase equilibria in the Cr-Ga-N system.* Materials Science and Engineering B, 1997. **49**(2): p. 152-154.

2. Farber, L. and M.W. Barsoum, *Isothermal sections in the Cr–Ga–N system in the 650–1000 °C temperature range.* J. Mater. Res., 1999. **14**: p. 2560-2566.

3. Barsoum, M.W. and L. Farber, *Room-Temperature Deintercalation and Self-Extrusion of Ga from Cr2GaN.* Science, 1999. **284**(5416): p. 937-939.

4. Chapter 4 Electrochemical Performances

In order to investigate electrochemical properties of Cr-Ga-N materials, several appropriate GaEx and CGN samples were selected and tested electrochemically. Assuming that ternary compounds in Cr-Ga-N system such as Cr_2GaN and Cr_3GaN uptake certain lithium atoms per 1 unit of each compound, theoretical values of electrochemical capacity were calculated. Based on these values, current rates were also calculated and applied to the corresponding samples. Experimental values of electrochemical capacities obtained from the tests were compared with these theoretical values of capacity retention. Electrochemical lithium intercalation/deintercalation tests were performed also on GaN, Cr_2N+CrN and Ga_2O_3 as contrast experiments in order to see if any of these compounds contributed to the reactivity of our samples toward Li. All battery test results were analyzes in terms of electrochemical capacity retention, voltage curve shape and reversibility. In the last section of this chapter, we proposed several reaction mechanisms for certain samples and deduced under which reaction each phase in Cr-Ga-N system underwent. Argument regarding possible reaction mechanisms was made based on the experimental results of *ex-situ* XRD along with Reitveld refinement analysis as well as electrochemical test results.

4.1 Experimental procedure

Cell assembly

Several GaEx and CGN powders prepared earlier were selected and tested for their

electrochemical performances vs. Li in Swagelok-type cells assembled in an argon-filled glove box, with oxygen and water contents below 5 ppm. After synthesis, the samples were ground in a mortar and mixed with Kynar as a binder and NMP as a solvent to dissolve the binder. This mixture was spreaded out uniformly on Cu foil using casting tools. Then, samples cast on Cu foil were put to stay in vacuum oven at 80 ℃ for overnight in order to remove the solvent (NMP). When dried out, electrode materials on copper foil were cut into pieces of certain square shape. This comprised working electrode and Li metal (lithium foil, 0.75mm of thickness) was used as counter electrode. The electrolytes we used consisted of 1.33 $LiPF_6$ in a 4:1:3:2 volume ratio mixture of EC, PC, DMC, and EMC. A microporous polypropylene film of Celgard 2400 was used as a separator. The cells were tested in a galvanostatic mode at various current rates. Current rates were calculated based upon the actual weight of active materials of electrodes. Since the electrodes were composed of Cu foil, powders of interest, and binder, the weight of Cu foil and binder was subtracted from the total weight of electrodes, giving us the actual weight of active materials. Based on active material weight, theoretical current rate was obtained by calculation and applied the samples appropriately.

X-Ray Diffraction (XRD)

Later in this chapter, we proposed several possible reaction mechanisms for each phase in Cr-Ga-N system. In order to verify if structure underwent expansion or contraction during cycling, *ex-situ* XRD was undertaken, providing information about unit cell parameter variation during cycling. The analysis of *ex-situ* XRD was made using

Reitveld refinement method.

4.2 Results and Discussion

4.2.1 Electrochemical performance of Cr-Ga-N materials

GaEx samples

In voltage profile of GaEx samples, there were three voltage plateaus shown both upon discharge and charge. (Figure 4.1) The voltage-capacity curves of GaEx samples greatly resemble the voltage-composition curve of Li-Ga alloys (Fig. 4.2) in that there are three distinct voltage plateaus located at similar height on charge and discharge, respectively. As published in reference [1], J. Saint et al. synthesized Li_xGa_y alloys such as Li_2Ga and LiGa by ball-milling Ga ingot and lithium powder and tested these alloys in Li-half cells potentiostatically. By comparison, we could see that both Li_xGa_y alloys and GaEx samples showed three distinctive voltage plateaus both on discharge and charge at similar height of voltage in capacity vs. voltage curves. (Figure 4.1 and Figure 4.2) This indicated that Li_xGa_y alloys and GaEx sample have similar activity toward Li. In chapter 3, by calculation, we confirmed that gallium metal comprised at least 45 % of the total sample weight. The existence of quite an amount of gallium metal in GaEx samples as well as the similar voltage profile shape of GaEx samples to Li-Ga alloys strongly suggested that the main electrochemically active material was gallium metal in GaEx samples. In terms of capacity retention, sample GaEx exhibited 182.87 mAh/g and 168.08 mAh/g on discharge and charge, respectively during the first cycle, followed by

the capacity value, 170.07 mAh/g and 163.70 mAh/g on discharge and charge, respectively in the second cycle. By definition, the first-cycle irreversibility is the difference between first-charge and first-discharge capacity, arising when lithium is trapped in the anode or is consumed irreversibly in a side reaction during the first cycle. As shown in chapter 1, a number of possible anode materials suffer from the large first-cycle irreversibility. Therefore, it is remarkable that GaEx samples displayed relatively low first-cycle irreversibility. (Table 4.1) The reversibility around 92.3% was obtained from GaEx 2 sample during the 1^{st} cycle. Although 1:1 molar ratio of gallium pellets and Cr_2N were put to attempt to synthesize Cr_2GaN, GaEx 6-8 samples were found to still contain gallium metal in the resulting powders, based on voltage profiles of these samples. The voltage-capacity curve of GaEx6-8 exhibited the same shape as the voltage profile of GaEx 1-5. The voltage profile and capacity-cycle number graph were depicted in Figure 4.3. It implied that although peaks of gallium metal were not detected in XRD patterns, the existence of gallium seemed obvious in all GaEx samples and the electrochemical capacity seemed to come from gallium metal remaining in GaEx samples remaining from the starting materials.

In addition, in order to see the effect of kinetics on GaEx samples, tests with reduced size particles (or amorphous phase) by milling and at higher temperature (at 37 ℃) were conducted. As shown in Figure 4.3, with increasing temperature conditions, electrochemical capacity increased by 40-50% and this demonstrated the kinetic influence upon reactions. Unlike high temperature test that didn't affect the shape of voltage profile, test results after milling the sample showed definite change in the shape of voltage profile as well as increasing values in electrochemical capacity.

Disappearance of step-wise plateaus in voltage profile implies either that through milling, amorphous phase or new phase were formed, or that reduced particle size of gallium or other materials behaved differently from the bulk sample at some point.

Table 4.1 Electrochemical capacity values of GaEx2

		cycle 1	cycle2
C/100	discharge	182.87	170.07
	charge	168.08	163.7
C/50	discharge	120.25	112.01
	charge	110.78	110.73

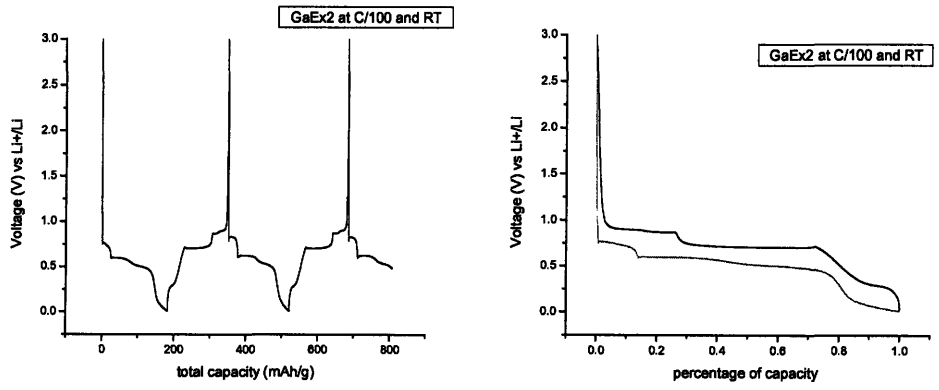

Fig. 4.1 **Voltage-capacity curve of GaEx 2 (left) and voltage-percentage of capacity curve of GaEx 2 during the first cycle (discharge in red line and charge in black line) (right)**

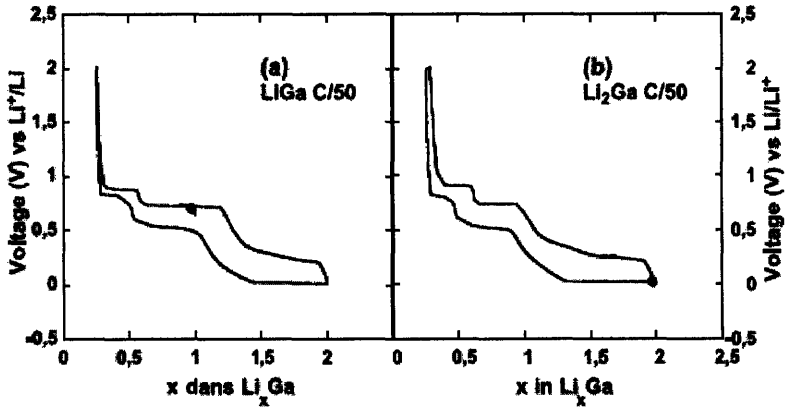

Fig. 5. Voltage composition profiles for (a) LiGa/Li and (b) Li_2Ga/Li cells. The cells were cycled at a rate of Li/50 h in the potentiostatic mode.

Fig. 4.2 **Voltage composition profile for LiGa/Li and Li_2Ga/Li.**

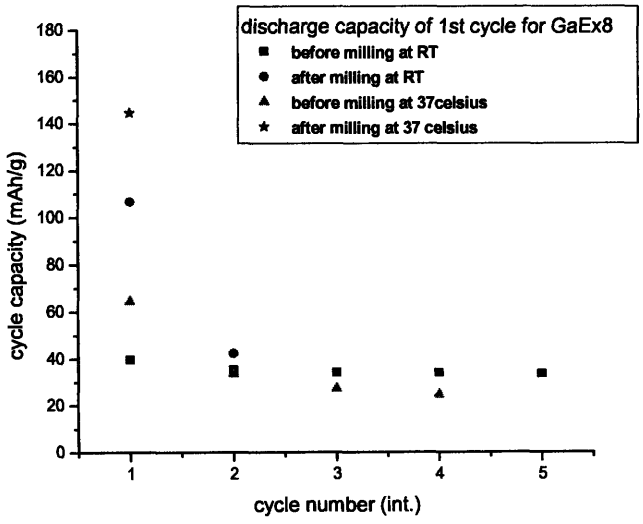

Fig. 4.3 **cycle capacity vs. cycle number of GaEx 8 (before milling and GaEx 9 after milling) tested at room temperature and 37 ℃**

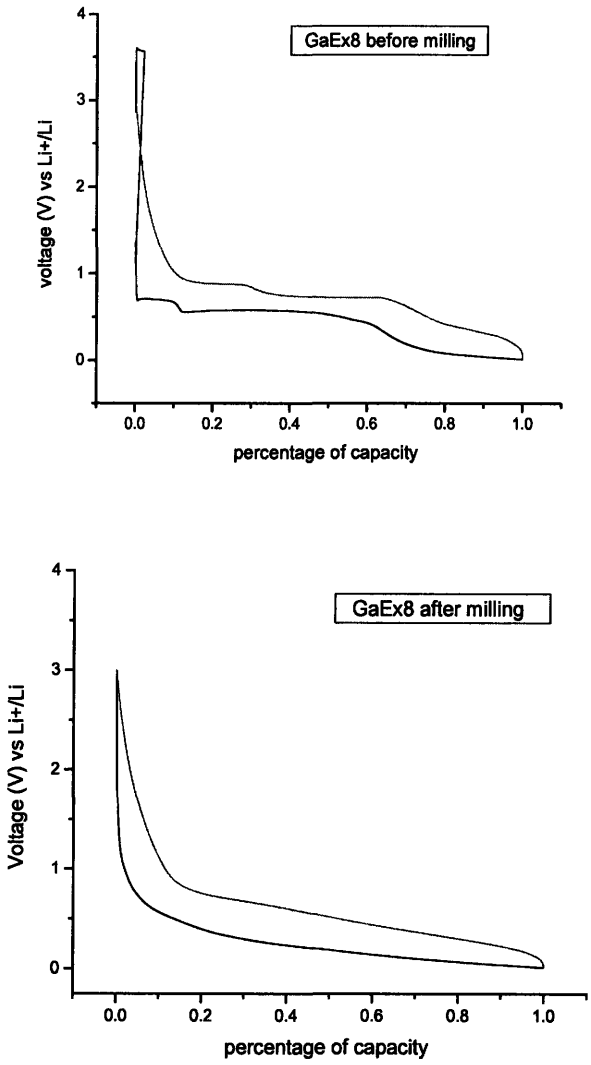

Fig. 4.4 Voltage-capacity curve of GaEx 8 before milling (up) and after milling (bottom)

CGN samples

After electrode casting, XRD was run on CGN samples before electrochemical tests. As illustrated in Figure 4.5, due to the unavoidable exposure to air even for a short time during electrode casting procedure, chromium oxide were formed and detected in XRD. As will be mentioned later in this chapter, these oxides were regarded to take active role mainly when the CGN samples reacted with lithium.

First of all, electrochemical test results of CGN5 (Cr_3GaN + oxides) were shown in Figure 4.6 In voltage-capacity profile, upon the first cycle discharge, one very flat monatomic curve continued from around 0.07V to 0.01V (limit voltage) instead of several level of step-wise plateaus that were seen in gallium active samples (GaEx's). This suggested that a reaction of different mechanism from that of LixGa alloy underwent in the reaction of CGN5 with lithium. In subsequent cycles, curves having certain inflections around 0.2V and 0.34~0.31V appeared quite reversibly. Considering electrochemical capacity retention values and the shape of voltage capacity profile, it implied that certain reactions occur quite reversibly after the first cycle. The theoretical capacity of Cr3GaN is 111.82 mAh/g and 223.64 mAh/g for 1 lithium uptake per 1 unit of Cr3GaN and 2 lithium uptake, respectively. Actual discharge capacity value of CGN5 exhibited 50.6575 mAh/g on discharge and 27.6503 mAh/g on charge, respectively at C/300 and room temperature during the first cycle.

One of the methods to check out the polarization effect is to test sample at different rate of current. Even though both are quite slow current rate, the current rate of C/300 and

C/100 were applied to CGN5 in order to see if there is any polarization occurring upon reaction in CGN5. (Figure 4.7) The difference between the electrochemical capacities from relatively lower and higher current tests gradually decreased and disappeared only after several cycles. Voltage profiles upon 1st cycle from both current condition tests were rescaled with respect to the percentage of cycle capacity of each test. From this comparison plot, we could see that lower current test exhibited a curve with a little more slope followed by a little lower plateau as current varied. However, little difference implied that not much polarization occurred in CGN5.

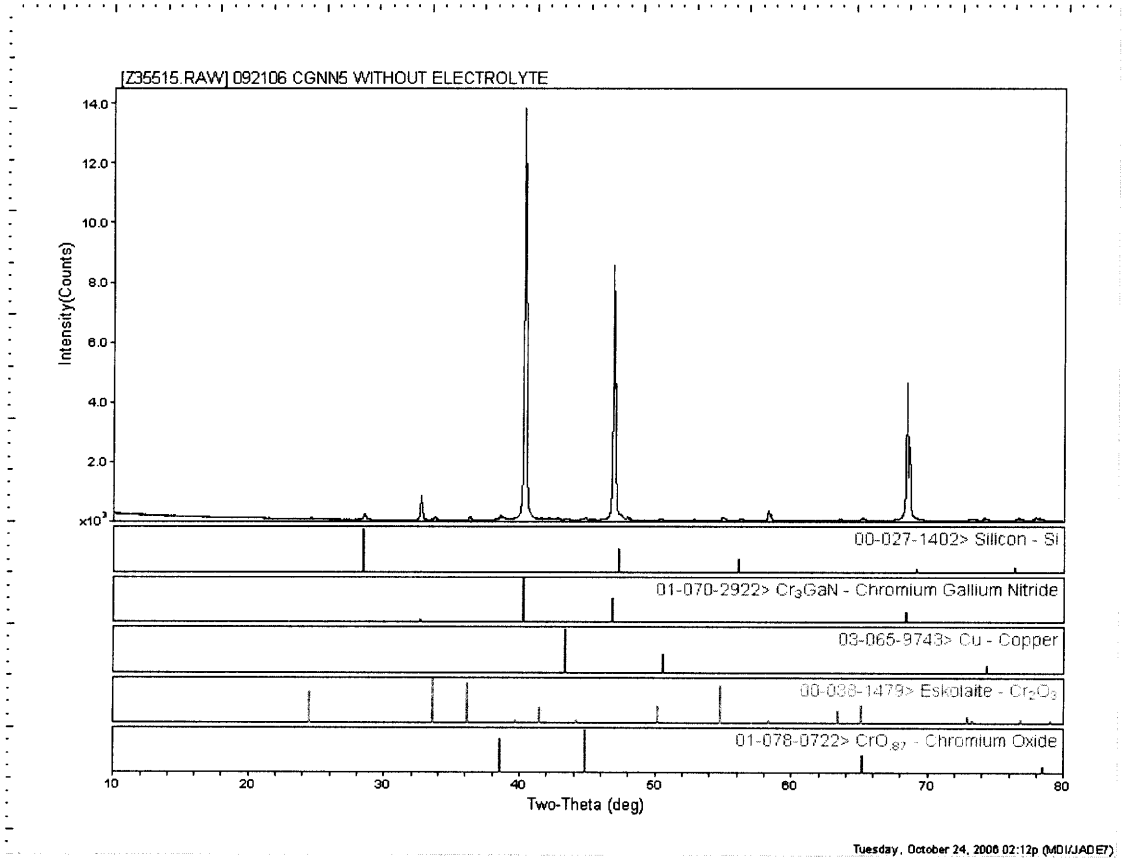

Fig. 4.5 **patterns of CGN5 after electrode casting**

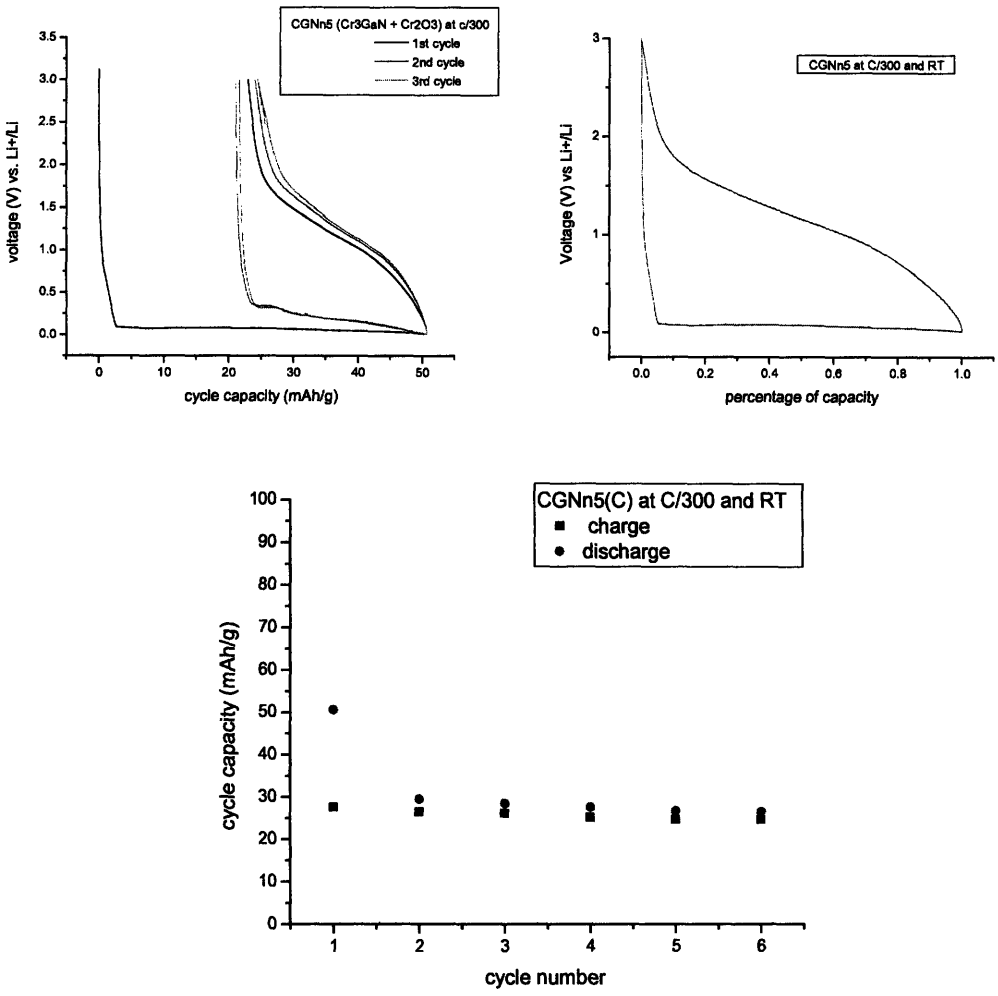

Fig. 4.6 Electrochemical test result for CGN 5. (a) Voltage-capacity curve, (b) voltage profile during the 1st cycle, and (c) cycle capacity

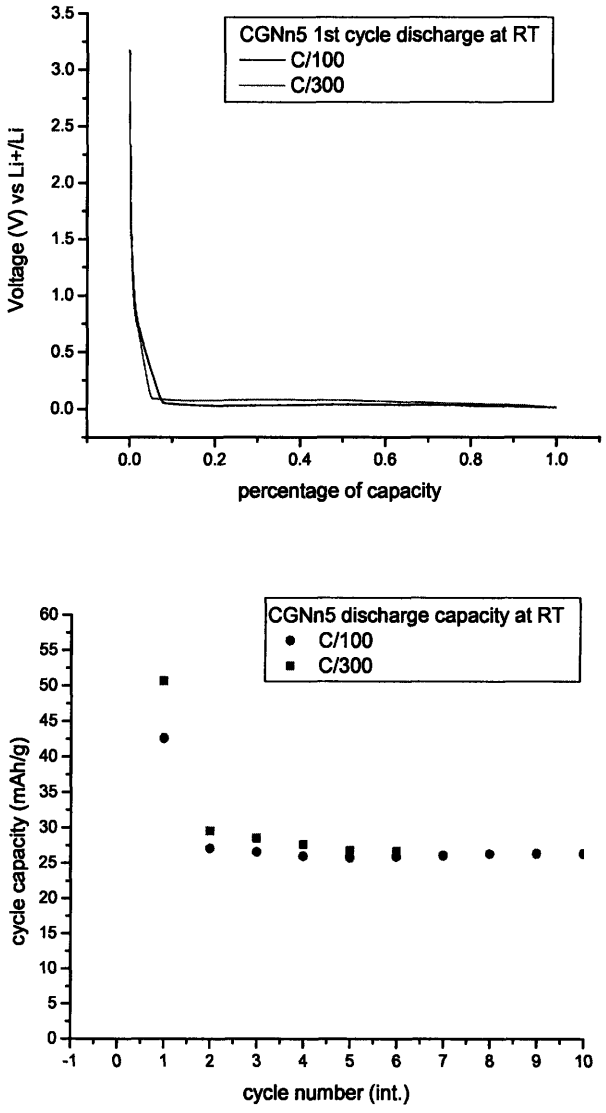

Fig. 4.7 Electrochemical test results for CGN5 at different current rate

Electrochemical tests were also conducted on CGN9 that was composed of Cr_2GaN as the first main phase, Cr_3GaN as the second main phase and oxides. (Figure 4.8) Theoretical capacity of Cr_2GaN is 142.794 mAh/g, assuming that 1 Li is inserted into 1 unit of Cr_2GaN. For two Li insertion per 1 unit of Cr_2GaN, the theoretical capacity of Cr_2GaN is 285.5879 mAh/g. The actual capacity of CGN9 during the 1^{st} cycle was 73.85 mAh/g on discharge and 47.78 mAh/g on charge, respectively. Similar to the voltage profiles of Li_xGa_y and GaEx samples, several step-wise curves were observed in CGN9 even though the length of voltage plateaus along capacity axis (or composition axis) was shorter. In order to compare LixGay alloys, GaEx2, and CGN9, the numbers of voltage from where voltage plateaus appeared in each sample are listed as follows:

Li_xGa_y upon discharge: 0.025 /0.52 /0.82V

GaEx2 upon discharge: 0.01-0.12 /0.50 and 0.59V /0.73V

CGNn9 upon discharge: 0.01-0.13V/ 0.46V /0.78V (1^{st} cycle) followed by 0.2V /0.47V (from the 2^{nd} cycles)

Although where voltage plateaus appeared in voltage profile of CGN9 seemed to correspond to GaEx2 (gallium excess sample), from a perspective of length of each plateaus along the capacity axis, obvious difference was shown between these two. These figures were also used to deduce the possible reaction mechanism of CGN9, especially Cr_2GaN phase later.

The tests at different current rate were undertaken on CGN9 also in order to see if any polarization occurred. (Figure 4.9) Unlike CGN5 where a bit of polarization observed,

both test results of CGN9 at C/300 and C/100 almost corresponded to each other in terms of voltage profile and cycle capacity values. Here, voltage profiles were re-plotted with modified scale, that is, percentage of each capacity for comparison. Although both C/300 and C/100 were slow current rates, polarization seemed not to occur at least at these two different rates in CGN9.

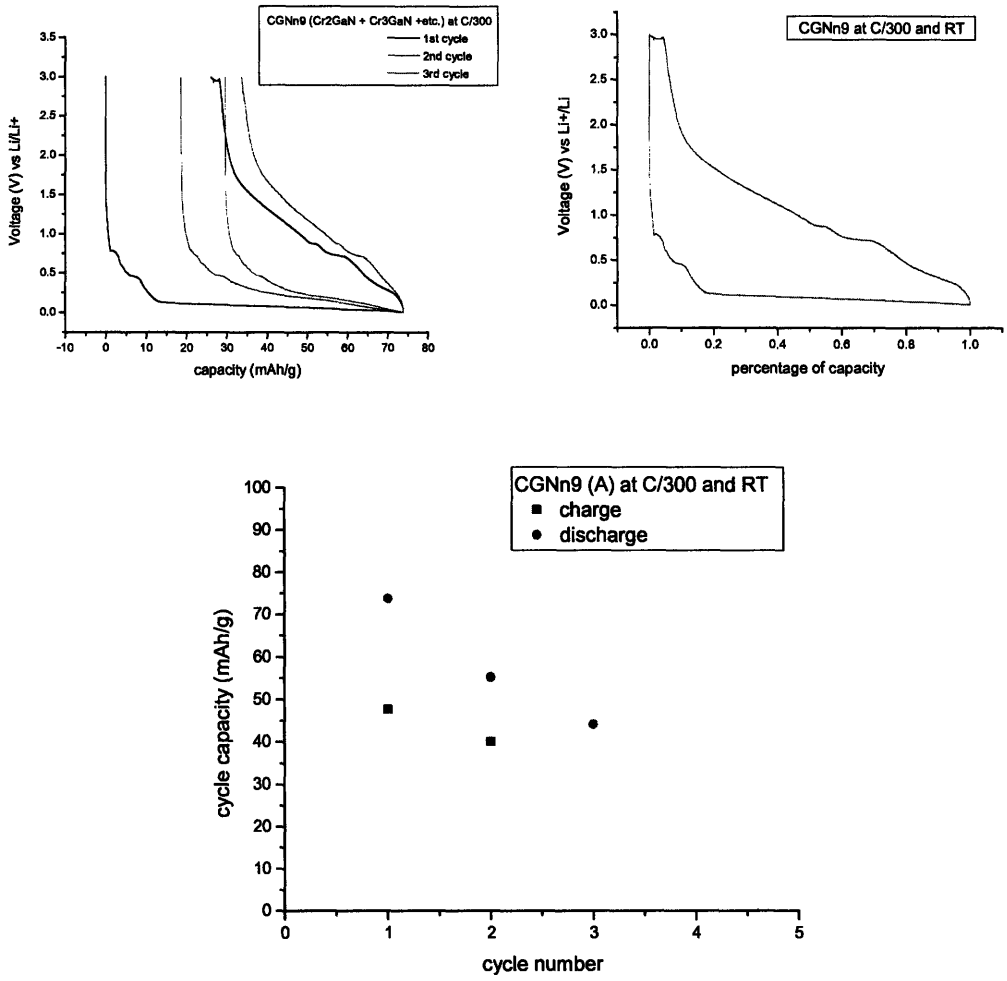

Fig. 4.8 Electrochemical test results of CGN9. (a) Voltage-capacity curve, (b) voltage-percentage capacity curve in the 1st cycle, and (c) cycle capacity vs. cycle number

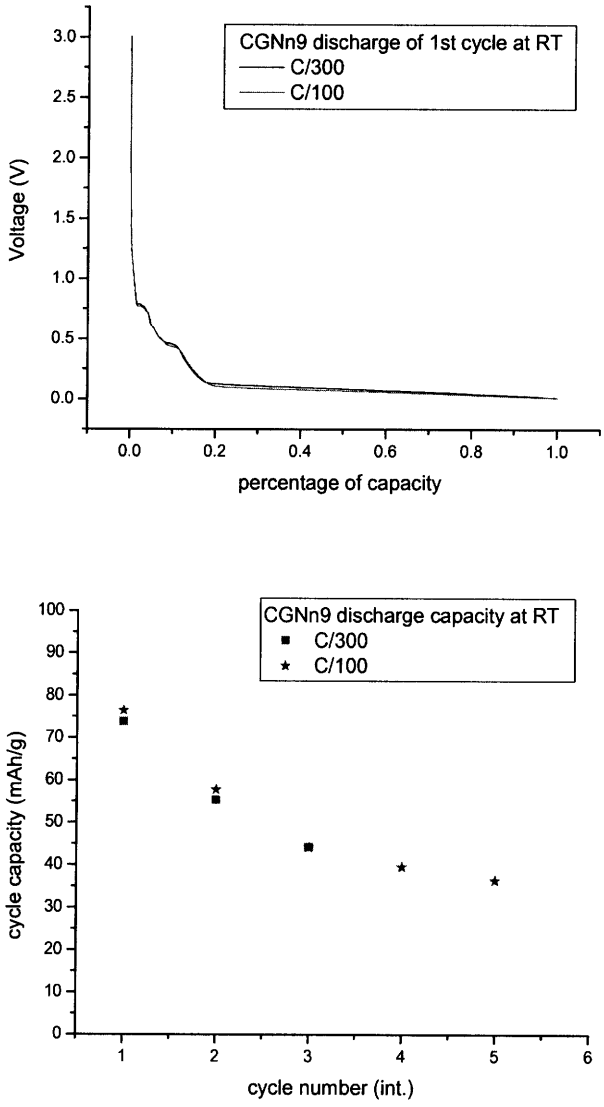

Fig. 4.9 **Electrochemical test results of CGN9 at different current rates**

4.2.2 Possible reaction mechanisms of Cr-Ga-N materials

In chapter 4.2.1, we presented how much lithium is taken up upon discharge/charge along with the corresponding voltage profile upon cycling, depending on each sample from different synthesis results. In this section, we extended our discussion to possible reaction mechanisms that occur during charge and discharge processes of each sample. Knowing how lithium insertion/deinsertion takes place would be of great help not only to understand the material itself more fundamentally but also to find out the way to improve the material properties as electrodes.

Reaction of GaEx 2 vs. Li

Earlier, it was shown that the main active material that stored lithium in GaEx2 was gallium metal even though the peaks of gallium didn't appear in the XRD patterns. The reaction mechanism of GaEx vs. Li, therefore, could be thought to follow the same mechanism as gallium metal or Li-Ga alloy, unless there was some other unknown component exhibiting similar voltage characteristics upon cycling to gallium. Provided that the argument regarding Li-Ga alloy reaction mechanism made by J. Saint et al. in reference [1] is quite reasonable, it can also be expected that the phase transitions of $Li_2Ga \Leftrightarrow LiGa \Leftrightarrow Li_2Ga_7$ also correspond to each voltage plateau of the GaEx samples. When compared to the voltage plateaus of similar position in Li-Ga alloy, the much shorter length of voltage plateau along composition axis at around 0.05V on discharge (0.28V on charge) indicated that the transformation from LiGa to Li_2Ga might be bypassed in GaEx samples due to slow reaction kinetics. As shown in Figure 4.10, a

phase transition of from LiGa to Li_2Ga is a structural transition from three dimensional structures to two dimensional structures that should entail atomic bond breakage and rearrangement. This means that a reaction of this kind is not likely to take place easily unless enough kinetic conditions such as high temperature and slow current rates are satisfied.

Besides, thorough voltage profile comparison between Figure 4.1 and 4.2 implied that more difference existed between pure Li-Ga alloy vs. Li reaction mechanism and the reaction of GaEx2 vs. Li although they had gallium metal in common as the electrochemically active component. First of all, unlike Li-Ga alloy case, very obvious inflection appeared at the second voltage plateau (0.5V and 0.59V) on discharge in GaEx2. According to phase diagram, the phase transition from Li_3Ga_2 to LiGa was possibly to occur in Li-Ga binary alloy reaction mechanism. It is suspected that the transition of from Li_3Ga_2 to LiGa also possibly underwent at around 0.59 V before the inflection, followed by the transformation from LiGa to Li_2Ga_7 at around 0.5V. Another difference is that voltage plateaus of GaEx systems are a little lower than pure Li-Ga alloy systems, especially on discharge. Possible reasons can be thought of regarding these differences between Li-Ga alloys and GaEx samples. GaEx samples were composed of not only gallium but also other phases unlike Li-Ga alloys, and therefore, the main active material, gallium in GaEx samples were surrounded by other phases. In the GaEx samples, there were other phases than gallium metal such as Cr_2GaN, Cr_3GaN and unreacted Cr_2N from starting raw material. Although the amount of each of these phases seemed relatively too small to take active role in reaction with Li compared to gallium metal, it could be plausible that these other phases, especially hard material,

Cr_2N, possibly kept its structure and helped conserve the system during cycling as TiC or SiC worked as a buffer matrix in Si-TiC or Ti-TiC nanocomposite materials [2]. The effect of different surrounding composition might be the reason as well why the capacity retention of GaEx system unusually reaches up to 92% upon cycling, while pure Li-Ga binary alloys still suffered from large irreversibility.

Possible Reaction Mechanism of CGN5 (Cr3GaN + oxides) vs. Li

In general, there are 2 types of reactions of Li with electrochemical active compounds: intercalation reaction and displacement reaction. From this point of view, several possible mechanisms were proposed, based upon experimental results and analysis.

i) Intercalation Reaction

Since CGN5 was mainly composed of the Cr_3GaN phase, an intercalation reaction of Cr_3GaN phase like below would be plausible.

$$xLi + Cr_3GaN \Leftrightarrow Li_xGa_3GaN \qquad \text{(Equation 4.1)}$$

If CGN5 underwent this intercalation reaction, Cr_3GaN structure should be expanded upon lithiation. In order to check the expansion or contraction upon lithiation, *ex-situ* X-ray experiment at several points of discharge of CGN5 during the first cycle was performed and analyzed through Reitveld refinement. The unit cell parameter variation

of Cr_3GaN structure upon 1st cycle discharge is presented in Table 4.2 along with goodness of fit (GOF). Typically, up to the third decimal point of unit cell parameters should be taken into account in Reitveld refinement. This table suggested that no systematic expansion or contraction of Cr_3GaN structure was shown and therefore, CGN5 sample did not undergo through an intercalation reaction of Cr_3GaN.

In JCPDS card available, $Cr_3GaN_{0.5}$ has been reported to have perovskite structure. Compared to perovskite Cr_3GaN, this phase is deficient in N atoms and therefore, the vacant sites of N atoms could be available for lithium ion to be inserted. Yet, since perovskite Cr3GaN is partially ionic, the idea of inserting more lithium cations into anion-deficient structure is too radical to be realized.

ii) Displacement Reaction of gallium

$$xLi + Cr_3GaN \Leftrightarrow Li_xGa_y + Cr_3Ga_{1-y}N \qquad \text{(Eqaution 4.2)}$$

This reaction is actually what we expected to happen in Cr_2GaN vs. Li, based on recent report that gallium was extruded from Cr_2GaN under particular circumstances. [3] Yet, little trace of Li-Ga compound either in XRD pattern or in voltage profile shape was found in *ex-situ* XRD patterns of Cr_3GaN upon lithiation. Taking into consideration that the perovskite structure is partially ionic cubic, we could imagine that the partially bonding of gallium atom with N atoms in this structure is not likely to part easily and alloy with Li.

iii) Displacement Reaction of nitrides

In several cases reported lately (i.e. Zn_3N_2, Cu_3N, Ge_3N_4) [4-7], nitrides, in general, exhibit the following 2-step reaction:

i) $M_xN_y + 3yLi+ + 3ye- \Leftrightarrow xM + yLi_3N$ (matrix) ---- irreversible reaction (Equation 4.3)

ii) $x\,M + z\,Li+ + ze- \Leftrightarrow Li_z M_x$ ----------reversible reaction (Equation 4.4)

If we apply this to Cr_3GaN phase,

i) $Cr_3GaN + 3yLi+ 3ye- \Leftrightarrow Cr_3Ga + Li_3N$ (Equation 4.5)

ii) $Cr_3Ga + zLi+ + ze- \Leftrightarrow Li_3Cr_3Ga$ (Equation 4.6)

Upon Li insertion, very minor peaks of assumed Cr_3Ga were shown a bit but little of Li_3N exists. In the literature, when nitrides follow the reaction mechanism above, the product, Li_3N peaks evolve very evidently with high intensity.

iv)Displacement reaction of oxides

If Cr_3GaN did not mainly contribute to the capacity of CGN5 vs. Li, it might be possible that oxides that were inevitably formed during the electrode casting process behaved as active species in reaction of CGN5 vs. Li. The plausible oxide phases are Cr_2O_3 and Ga_2O_3 as confirmed in XRD patterns. (Figure 4.5) Electrochemical

performance of Cr_2O_3 has already been studied by other research group. [8] (Figure 4.11) According to Jin et al., Cr_2O_3 was known to undergo similar reaction mechanism of oxides to the one of TMO (tin metal oxide) like below:

$$Cr_2O_3 + 6Li \rightarrow 2Cr + 3Li_2O \qquad \text{(Equation 4.7)}$$

In their experiments, the initial discharge capacity reached up to 1166 mAh/g, which was larger than the theoretical value of 1058 mAh/g, owing to extra Li storage in SEI formation. The initial charge capacity value was 771 mAh/g, showing irreversibility as other metal oxides do.

As no report on the electrochemical properties of Ga_2O_3 has been found, galvanostatic test was conducted with commercially available Ga_2O_3 in this work. Based on several aspects of voltage-capacity curve and cycling behavior (Figure 4.12), it can be concluded that Ga_2O_3 features the typical displacement reaction behavior of metal oxides [9-13]. The first discharge plateau was continuously flat line, which indicated high capacity, followed by a charge plateau with less capacity. The second discharge appeared at higher voltage but there still exists polarization, providing charge plateau with less capacity than discharge capacity. Subsequent cycles are in the same pattern as the 2nd cycle except for capacity loss. This typical metal oxide voltage behavior suggests 2-step reaction mechanisms:

1st discharge: $Ga_2O_3 + 6Li \rightarrow 2Li_2O + 2Ga$ (irreversible) (Equation 4.8)

2nd and further discharge: $xLi + 2Ga \Leftrightarrow LixGay$ (reversible) (Equation 4.9)

Another common feature of metal oxide also displayed in Ga_2O_3 is that experimental capacity value of 1200 mAh/g is much larger than the theoretical capacity value of 858 mAh/g, storing 6Li per unit Ga_2O_3. In short, both Cr_2O_3 and Ga_2O_3 turned out to be one of typical metal oxides that generate large irreversible capacity initially with low flat voltage plateau, followed by relatively reversible capacity retention.

Now, whether these oxides are the major active species in CGN5 sample should be answered. There are several supporting bases. First of all, the voltage curve and cycle capacity of CGN5 (Figure 4.6 and Figure 4.7) resembled the behavior of metal oxides of Cr_2O_3 and Ga_2O_3 (Figure 4.11 and Figure 4.12). Upon 1st cycle discharge, one very flat monotomic curve continued from around 0.07V to 0.01V (limit voltage). In the following cycles, curves having certain inflections around 0.2V and 0.34~0.31V appeared quite reversibly. When electrochemical capacity retention and voltage-capacity profile were considered, certain reactions seemed to occur quite reversibly after an irreversible reaction during the 1st cycle. In addition, although the intensity of oxides peaks were not strong compared to the main phase Cr_3GaN in the XRD patterns due to small amount, when the part where oxide peaks appeared upon lithiation were magnified for the sake of analysis, it was observed that the peak intensities of oxides were decreasing upon lithiation, implying consumption of oxides upon Li uptake. Lastly, by calculation, it is proved that only 0.083 wt% of total sample material weight should belong to oxides in order to provide about 30 mAh/g, which was the actual capacity value of CGN5 in our work. Thus, it seemed also reasonable that product such as Li_2O from the reaction of oxides with Li were weakly detected only in *ex-situ* X-ray

experiment upon lithiation even though oxides take the active role in the mechanism.

Possible reaction mechanism of CGN9 vs. Li

It was useful to compare voltage profiles of GaEx2, CGN5 and CGN9 in the same plot so that bigger picture about the possible mechanism can be captured. The 1st discharge and charge voltage curves are re-drawn along the percentage of each capacity all together in Figure 4.13. Above all, the behavior of CGN9 stood out in that its voltage profile looked like a combination of the other two voltage profiles. There were noticeable steps in the voltage plateau curve of CGN9 like the step-wise voltage profile appeared in GaEx 2, but with different length and slope along the percentage of capacity axes. In terms of slope of voltage vs. capacity, the voltage-capacity curve of CGN9 rather resembled CGN5. The lowest and longest voltage plateau shown in the voltage-capacity curve of CGN9 also was almost consistent with the voltage-capacity profile of CGN5. If oxides were the only active species in CGN9 like CGN5, the voltage profile should have looked like the one of CGN5. There were, however, more detailed steps distinctly that were shown in the voltage-capacity curve of GaEx2. Even upon charge, the height where voltage plateaus were situated was consistent with gallium metal (GaEx2) vs. Li case. Furthermore, much more reversible capacity retention of was shown in CGN9 than in CGN5. This intermediate behavior suggested that in electrochemical reaction of CGN9 vs. Li, gallium in certain way (either from extrusion from Cr_2GaN structure or from remaining amorphous gallium) took an active role while, at the same time, other reactions such as displacement reaction of oxides from CGN5 occurred at the same time, generating mixing mechanism of reaction in CGN9. This

implied that not only displacement reactions of oxides took place but also that gallium, extruded from Cr_2GaN phase, underwent a displacement reaction in CGN9, both at the same time.

Table 4.2 Unit cell parameter variation of CGN5 upon lithiation

Voltage upon lithiation	Unit cell parameter (A)	Goodness of Fit (GOF)
Before discharge (3.00V)	3.875507	2.88
At 0.7 V	3.876876	3.39
0.1280V	3.875860	2.97
0.08V	3.876207	2.57
0.04V	3.876207	1.50
0.01V	3.875503	3.90

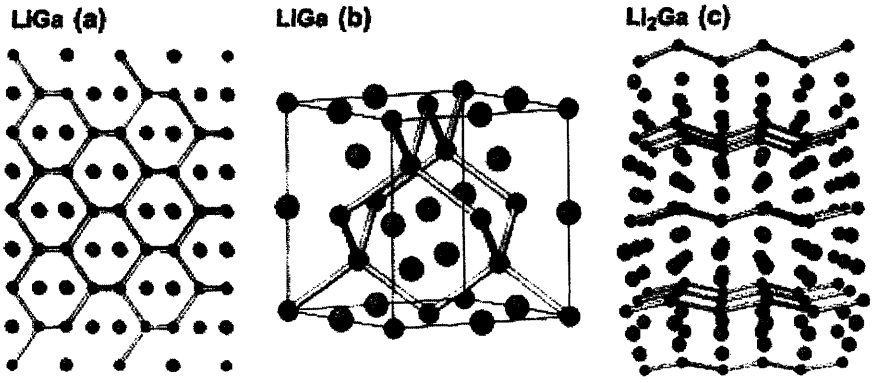

Fig. 4.10 The crystal structures of (a), (b) LiGa and (c) Li_2Ga.[1]

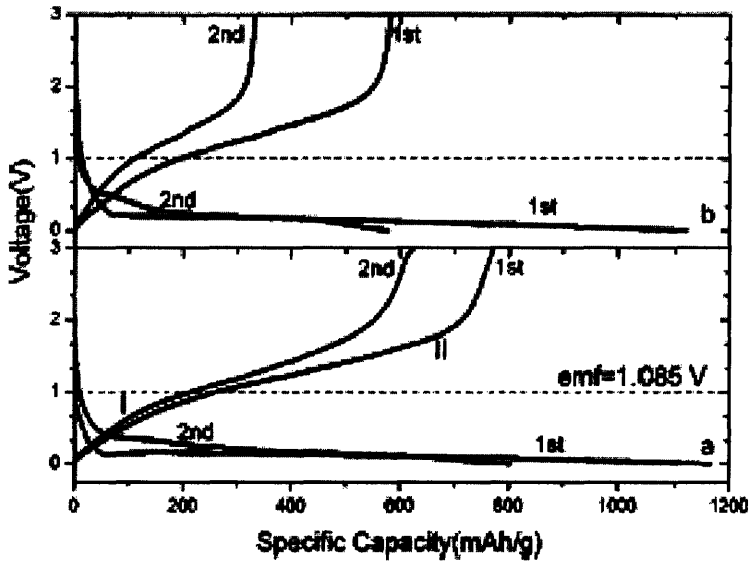

Figure 1. Charge-discharge curves of a Li/Cr_2O_3 cell at the first two cycles. (a) Electrode prepared with carbon black (10 wt %) and binder (5 wt %), and (b) electrode prepared without any additive. Roman numbers marked in the figure are explained in the text. Current density is 0.2 mA/cm^2.

Fig. 4.11 **Voltage-capacity profile of Cr2O3 [8]**

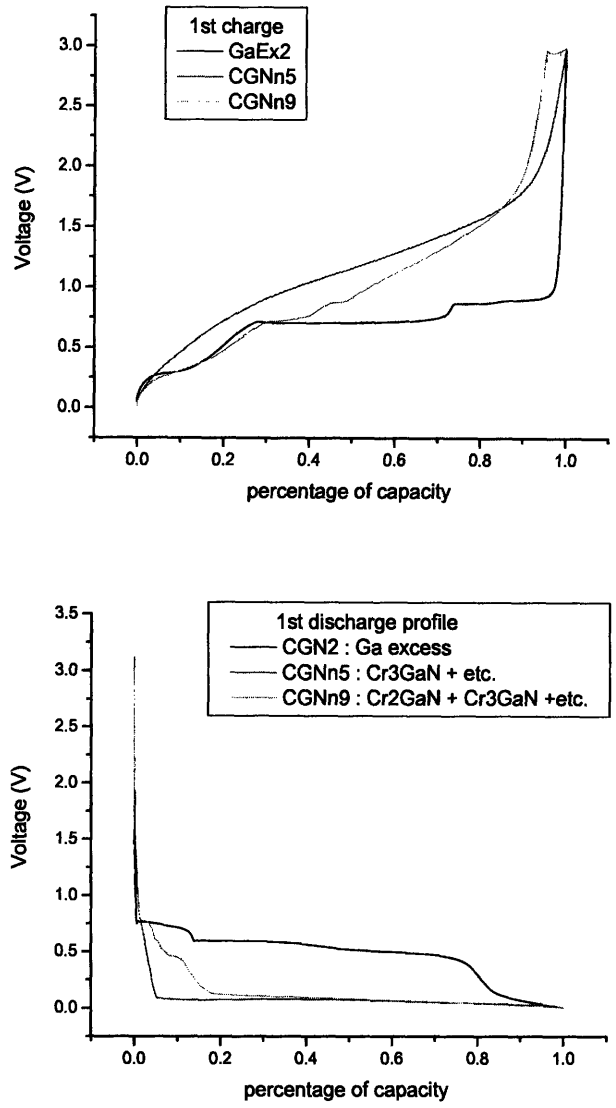

Fig. 4.12 **Voltage-percentage of capacity of GaEx2, CGN5, and CGN9 during the first cycle on the same plot**

4.3 References

1. Saint, J., et al., *Exploring the Li-Ga room temperature phase diagram and the electrochemical performances of the LixGay alloys vs. Li.* Solid State Ionics, 2005. **176**(1-2): p. 189-197.
2. Huggins, R.A., *Alternative materials for negative electrodes in lithium systems.* Solid State Ionics, 2002. **152-153**: p. 61-68.
3. Barsoum, M.W. and L. Farber, *Room-Temperature Deintercalation and Self-Extrusion of Ga from Cr2GaN.* Science, 1999. **284**(5416): p. 937-939.
4. Cabana, J., et al., *Oxynitrides as Electrode Materials for Lithium-Ion Batteries.* Journal of The Electrochemical Society, 2005. **152**(11): p. A2246-A2255.
5. Cabana, J., et al., *Antifluorite-Type Lithium Chromium Oxide Nitrides: Synthesis, Structure, Order, and Electrochemical Properties.* Inorganic Chemistry, 2004. **43**(22): p. 7050-7060.
6. Pereira, N., et al., *The Electrochemistry of Germanium Nitride with Lithium.* Journal of The Electrochemical Society, 2003. **150**(8): p. A1118-A1128.
7. Shodai, T., Y. Sakurai, and T. Suzuki, *Reaction mechanisms of Li2.6Co0.4N anode material.* Solid State Ionics, 1999. **122**(1-4): p. 85-93.
8. Hu, J., et al., *Improve the electrochemical performances of Cr2O3 anode for lithium ion batteries.* Solid State Ionics, 2006. **177**(26-32): p. 2791-2799.
9. Badway, F., et al., *Metal Oxides as Negative Electrode Materials in Li-Ion Cells.* Electrochemical and Solid-State Letters, 2002. **5**(6): p. A115-A118.
10. Courtney, I.A. and J.R. Dahn, *Key Factors Controlling the Reversibility of the Reaction of Lithium with SnO[sub 2] and Sn[sub 2]BPO[sub 6] Glass.* Journal

of The Electrochemical Society, 1997. **144**(9): p. 2943-2948.

11. Idota, Y., et al., *Tin-Based Amorphous Oxide: A High-Capacity Lithium-Ion-Storage Material.* Science, 1997. **276**(5317): p. 1395-1397.

12. Poizot, P., et al., *Electrochemical reactivity and reversibility of cobalt oxides towards lithium.* C.R. Acad. Sci. II, 2000: p. 681-691.

13. Poizot, P., et al., *Nano-sized transition-metal oxides as negative-electrode material for lithium-ion batteries.* Nature, 2000. **407**: p. 496-499.

Chapter 5 Conclusion

In summary, single phase materials of ternary compounds in Cr-Ga-N system such as Cr_2GaN and Cr_3GaN were hard to fabricate. Instead, in this work, samples composed of several kinds of Cr-Ga-N materials were obtained by weighing, mixing, cold isostatic pressing, vacuum sealing, and heat treatment. Electrochemical tests were conducted on several selected samples. Although electrochemical capacity of Cr_2GaN was found not to be large, observation that gallium from Cr2GaN structure seemed to be electrochemically active was notable. Possible reaction mechanisms for the individual samples were discussed, based on experimental data.